EUROPEAN ORGANIZATION FOR NUCLEAR RESEARCH
CERN - ACCELERATORS AND TECHNOLOGY SECTOR

CERN-ATS-2013-044

Superconducting Materials and Conductors : Fabrication and Limiting Parameters

Luca Bottura
CERN, Geneva, Switzerland

Arno Godeke
Ernest Orlando Lawrence Berkeley National Laboratory, Berkeley, USA

Superconductivity is the technology that enabled the construction of the most recent generation of high-energy particle accelerators, the largest scientific instruments ever built. In this review we trace the evolution of superconducting materials for particle accelerator magnets, from the first steps in the late 1960s, through the rise and glory of Nb–Ti in the 1970s, till the 2010s, and the promises of Nb_3Sn for the 2020s. We conclude with a perspective on the opportunities for high-temperature superconductors (HTSs). Many such reviews have been written in the past, as witnessed by the long list of references provided. In this review we put particular emphasis on the practical aspects of wire and tape manufacturing, cabling, engineering performance, and potential for use in accelerator magnets, while leaving in the background matters such as the physics of superconductivity and fundamental material issues.

Published in Rev. Accel. Sci. Technol. 5 (2012) 25-50

Geneva, Switzerland

February 2013

Reviews of Accelerator Science and Technology
Vol. 5 (2012) 25–50

DOI: 10.1142/S1793626812300022

World Scientific
www.worldscientific.com

Superconducting Materials and Conductors: Fabrication and Limiting Parameters

Luca Bottura
CERN, CH-1211 Geneve 23, Switzerland
luca.bottura@cern.ch
Arno Godeke
Ernest Orlando Lawrence Berkeley National Laboratory,
1 Cyclotron Rd., Berkeley, CA 94720, USA
agodeke@lbl.gov

Superconductivity is the technology that enabled the construction of the most recent generation of high-energy particle accelerators, the largest scientific instruments ever built. In this review we trace the evolution of superconducting materials for particle accelerator magnets, from the first steps in the late 1960s, through the rise and glory of Nb–Ti in the 1970s, till the 2010s, and the promises of Nb_3Sn for the 2020s. We conclude with a perspective on the opportunities for high-temperature superconductors (HTSs). Many such reviews have been written in the past, as witnessed by the long list of references provided. In this review we put particular emphasis on the practical aspects of wire and tape manufacturing, cabling, engineering performance, and potential for use in accelerator magnets, while leaving in the background matters such as the physics of superconductivity and fundamental material issues.

Keywords: Superconductors; LTS materials; HTS materials; superconducting cables; superconducting accelerator magnets.

1. A Perspective on Applied Superconductivity for HEP Magnets

High-energy physics (HEP) has been a strong driver in the development of technical superconductors. The potential of superconductors for HEP experiments became clear already in the early 1960s, when the groups at Bell Labs, Westinghouse, Atomics International, Lincoln Labs, and Oak Ridge Laboratories reached fields well above 2 T, the typical range of classical electromagnets. By 1961, fields of 6 T were achieved in solenoids using a cold-drawn Nb–Zr alloy by Hulm from Westinghouse and Richard Hake and Ted Berlincourt from Atomics International, and record values of 7 T were reported by John Eugene Kunzler, at Bell Labs [1], using a wire made of Nb tubes filled with crushed powder of Nb and Sn, and heat-treated at 1000°C to chemically react the precursors into Nb_3Sn [2].

The superconducting wires developed at that time had critical current densities in the range of a few hundred to a thousand A/mm^2, and could be employed to wind magnets of medium-to-large size used to produce, for example, the background field in a particle detector. The initial applications were plagued by flux-jump instabilities and required much ingenuity to achieve practical results. Swift progress in the technology, and an undeniable pioneering spirit, made it possible to achieve remarkable results. The most relevant examples are the large-size bubble chambers at Argonne National Laboratory [3–5], BNL [6], and the Big European Bubble Chamber at CERN [7], which, with a stored energy of 800 MJ, remained for some 35 years the largest-size single magnet ever built.

Various materials were considered in that early age. Cold-drawn Nb wires were the initial step toward large current-carrying capability [8, 9]. Mo_3Re and Nb_3Sn were the first high-field superconductors [10, 11], but their use did not find widespread application due to the difficulty inherent with the material brittleness, and large filaments. On the other hand, the earlier recognition of the effect of cold work and precipitates in Nb wires led to the development of Nb–Zr, the first commercially available

superconductor, and later Nb–Ti, which has become the material with the largest application basis, and undoubted success [12].

Indeed, Nb–Ti has been the workhorse for the vast majority of HEP applications. Multifilamentary Nb–Ti wires became widespread in the late 1960s and 1970s, while scientists understood the need for twisting and cabling [13, 14]. Different choices of cable configurations fueled the dispute between the Energy Doubler/Saver [15], known later as the Tevatron [16], and Isabelle [17], later christened the Colliding Beam Accelerator (CBA) and terminated by DOE in favor of the Superconducting Super Collider [18]. The SSC prototypes [18], the proton ring at the Hadron Electron Ring Accelerator (HERA) [19], the UNK prototypes [20], and the Relativistic Heavy Ion Collider (RHIC) [21] were all built using Rutherford-type cables made of multifilamentary Nb–Ti wires. The latest achievement is the Large Hadron Collider (LHC) [22], which will soon be pushing the operating field to the 8 T range, the practical boundary of Nb–Ti for this class of applications. The companion paper [23] contains an abridged history of the research and achievements in the field of superconducting accelerator magnets.

Similarly, Nb–Ti cables have found widespread application in the magnets providing the bending field for HEP detectors. The main advantage with respect to resistive electromagnets is the possibility of generating the desired magnetic field configuration and strength with a very thin winding, i.e. transparent to the particles to be detected and tracked. The first detector solenoids were built in the 1970s at the CERN ISR [24], PEP-4 at SLAC [25], and CLEO-1 at Cornell University [24]. A major technological advance was the Al-stabilized Nb–Ti conductor that was developed in the late 1970s at CEN-Saclay, for the CELLO detector solenoid at DESY [26]. The Al-stabilized conductor had the advantage of improved stability to external perturbations (see later), which is a very interesting feature when one is dealing with magnets of large size that are subjected to continuous radiation loads. This conductor, in a number of configurations, has found applications in all large HEP magnets built during the last 40 years, from CDF at the Tevatron [27], through ALEPH [28] and DELPHI [29] at LEP, to the most recent examples of ATLAS [30] and CMS [31] at the LHC. This last magnet, with a stored energy of 2.6 GJ, holds today the record for the single magnet with the largest stored energy.

At this point in time Nb–Ti has reached industrial maturity and is operating close to its intrinsic limitations (refer also to the later discussion). It is clear that it will be difficult, if not impossible, to surpass the latest achievements without resorting to new materials. To exemplify this situation, we report in Fig. 1 the evolution in time of the critical current density J_c of industrial Nb–Ti wires in the past 35 years. Throughout this article we define J_c as the ratio of the critical current I_c to the *non-stabilizer* area in the wire $A_{\text{non-stabilizer}}$:

$$J_c = \frac{I_c}{A_{\text{non-stabilizer}}}. \tag{1}$$

As heritage from LTS materials, the *non-stabilizer* cross section is commonly referred to as *non-Cu*, which is applicable to Nb–Ti and Nb_3Sn, but no longer appropriate for HTS materials. We observe in Fig. 1 that the non-Cu critical current density at 5 T and 4.2 K was dramatically increased during the transition from the Tevatron production to the SSC R&D, in the 1980s (see also later). This gain was beneficial to industrial applications, foremost being MRI and NMR magnets, and was later exploited in the construction of the LHC. We see that the level achieved in the late 1980s has improved by as little as 10% over the past 20 years, which suggests that the full industrial potential of this material has been reached.

In the same plot we report the evolution of the critical current density of Nb_3Sn, which we believe is the material that will provide the next step in

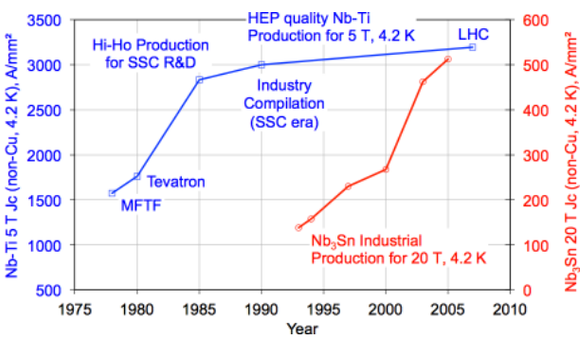

Fig. 1. Evolution of the critical current of industrially produced Nb–Ti (*left*) and Nb_3Sn wires (*right*). The critical current of Nb–Ti is quoted at 5 T and 4.2 K, for Nb_3Sn at 20 T and 4.2 K. (Data courtesy of J. Parrell, Oxford Superconducting Technology, Carteret, NJ, USA.)

superconducting accelerator magnets, measured at 20 T and 4.2 K. We note a jump in J_c in the early 2000s, which is the result of the Conductor Development Program (CDP) supported by DOE since the year 1999 [32]. This improvement was achieved thanks to the choice of optimal Sn content and non-Cu fraction. The record current density achieved in commercial wires in 2005 is still unsurpassed, while work focusses presently on other properties such as copper RRR, magnetization, stable production, and yield. This vigorous R&D is still ongoing to prove that Nb_3Sn is mature for HEP applications in the range of 15 T [33–35]. Results are expected by 2015, based upon which the production of the first Nb_3Sn accelerator magnets could start, for installation in the LHC in the early 2020s.

The classic low-temperature superconductors (LTSs) are only a part of the present landscape of commercial superconductors. Figure 2 shows the state-of-the-art current density in LTS and HTS materials of interest for magnet construction [36]; here the authors report the engineering current density J_E obtained as the ratio of the critical current I_c to the total cross-section of the conductor (strand or tape) $A_{\text{conductor}}$, including stabilizer, barriers, and structural or buffer materials:

$$J_E = \frac{I_c}{A_{\text{conductor}}}. \tag{2}$$

HTS materials have exceedingly high critical fields at low temperature, 4.2 K in Fig. 2, and they possess great potential as high-field superconductors. This potential can be exploited to push further the field in accelerator magnets, beyond the limit of about 18 T for Nb_3Sn. This target is being pursued by a number of companion programs worldwide [37, 38], targeting specifically the $Bi_2Sr_2CaCu_2O_{8+x}$ (Bi-2212) and $YBa_2Cu_3O_{7-\delta}$ (YBCO) class of cuprates. Results are expected on the horizon of 2015, by which time further demands from HEP may call for higher particle energies and larger accelerators.

In the meantime, the HTS materials have found a first large-scale use in the current leads of the LHC (Bi-2223). In the near future, HTS materials, as well as MgB_2, are considered for applications in superconducting bus bar cables in the LHC [40]. These superconducting links would allow placing the powering equipment, including power converters, control electronics, and possibly protection diodes, in zones that are well shielded from radiation. This application is a major scale-up of a concept realized using LTS materials, such as the bus powering the J-PARC combined function magnets at KEK [41]. With material demands in the range of thousands of kilometers, these power transmission applications provide a definite push for the industrialization of novel materials, which are still in their industrial infancy compared to Nb–Ti and Nb_3Sn.

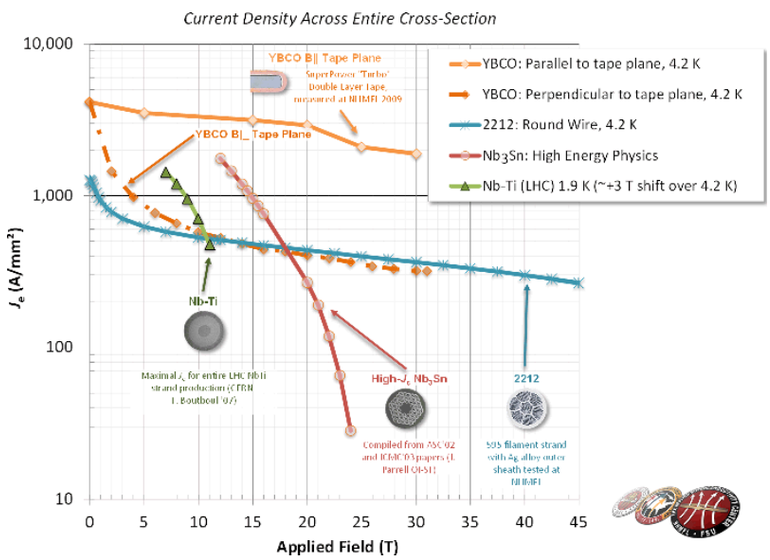

Fig. 2. State-of-the-art engineering current density for technical superconductors (at 4.2 K except for Nb–Ti, which is quoted at 1.9 K). (Data courtesy of P. J. Lee, Applied Superconductivity Center, NHMFL, Tallahassee, FL, USA.)

2. Relevant Parameters for Application in Accelerator Magnets

A *good* superconducting material must have a number of specific properties that make it suitable for practical accelerator magnet applications. They are listed and discussed below, with typical order-of-magnitude estimates based on common practice in accelerator magnet design and construction.

2.1. *Critical current density*

A practical and economical superconductor has a high critical current density and operating margins under the desired operating conditions of field and temperature. An efficient winding requires a coil current density J_{avg}, averaged over all coil components, in the range of 400–500 A/mm^2. Significantly smaller values result in coils that are too large and too costly [23, 42]. Much larger values in magnets producing the strong fields of interest here would yield mechanical stresses in the winding exceeding allowable levels for the superconductor, or other coil components such as the insulation, and may be difficult to protect in case of quench. The above target on J_{avg} can be translated in a typical requirement for the engineering current density in the superconducting wire or tape, i.e. J_E (defined earlier), or in the non-Cu fraction, i.e. J_c, by considering the processing of wires and the amount of material in a coil cross-section. Figure 3, which is an example for a Nb_3Sn cable, shows schematically the various material distributions.

Cabling a superconducting wire, e.g. in the form of a Rutherford cable described later, can induce a degradation of the critical current caused by heavy deformation of the filaments. Acceptable degradation is in the range of 5–10%. The void fraction of a Rutherford cable, combined with the space occupied by the cable insulation, further reduces the achievable current density in the windings by typically 30% for the wire in the cable, which means that, overall, the current density in the windings is reduced by about 35% when compared to the round wire before cabling. A required winding current density J_{avg} of about 400–500 A/mm^2 needs therefore an engineering current density J_E of about 600–800 A/mm^2 in the wire.

In a typical accelerator wire, the non-Cu fraction (i.e. the superconductor, as well as barriers, substrates, and residual from possible heat reactions) constitutes 50% of the wire cross-section. The

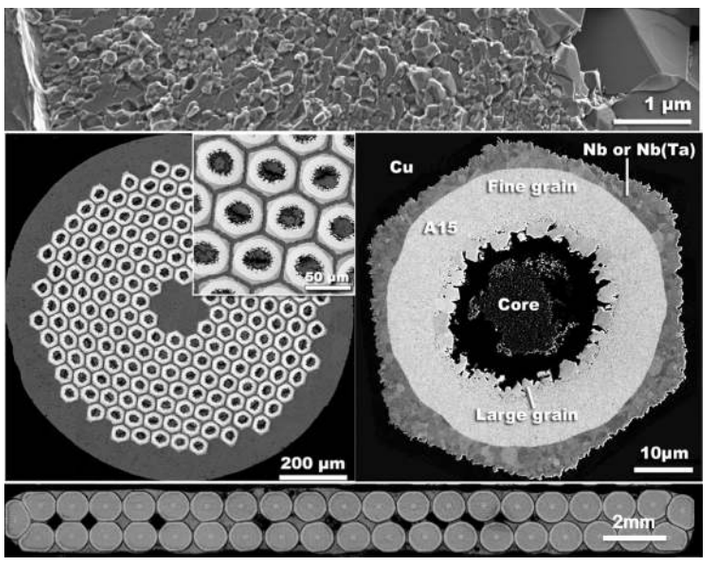

Fig. 3. Rutherford cable, wire, a typical filament cross-section of the non-Cu fraction, and a detail of the fine-grain volume in a powder-in-tube Nb_3Sn wire. The approximate cross-sectional fractions in the non-Cu area are: fine-grain Nb_3Sn — 40%; large-grain Nb_3Sn — 10%; core — 25%; and unreacted Nb or Nb–Ta — 25%. (Reproduced from Ref. 39; wire and filament images courtesy of P. J. Lee and C. M. Fisher, Applied Superconductivity Center, Tallahassee, FL, USA; cable image courtesy of L. Oberli, CERN, Geneva, Switzerland.)

requirement for J_c, which is defined here over the wire cross-section excluding the stabilizer fraction in accordance with the common convention, is thus about 1200–1600 A/mm^2. Finally, as shown in Fig. 3, only a fraction of the non-Cu cross-section may be superconducting, depending on the specific material. In the example shown there, a powder-in-tube (PIT) Nb_3Sn wire, it is seen that the fine-grain Nb_3Sn volume, which carries the superconducting current, amounts to about 40% of the non-Cu cross-section, and thus only about 20% of the total wire cross-section. The requirement for the current density in the superconducting fraction, or J_{SC}, is therefore of order 3000–4000 A/mm^2, which is available in modern Nb_3Sn wires up to about 15 T at 4.2 K [43].

The above ranges for J_E and J_c are good guidelines for estimating the magnetic field reach of a given material. As an example, we see, examining the plot in Fig. 2, that Nb–Ti is suitable for applications up to 10 T at 1.9 K, while Nb_3Sn extends this reach to 16 T at 4.2 K, which agrees with the achieved dipole magnetic field records [44, 45]. It should be noted that in large-scale applications the magnets will not be operated so close to their limits, and that a typical margin of about 20%, measured along the magnet *load line*, is commonly observed. HTS materials are approaching the range of practical interest, but still require an improvement of J_E by a factor of 3–4 (Bi-2212; Sec. 4), or an increase in the superconducting fraction and/or a reduction in the anisotropy (YBCO; Sec. 4) to become effective in a compact magnet, and enable the magnetic field range to be extended beyond the performance of the classic LTS conductors.

2.2. *Stabilizer*

The superconducting material must be compatible with a high-electrical-conductivity material (the most common material is Cu, but Al and Ag are also used), to be placed in intimate electrical and thermal contact with the superconductor itself. This so-called *stabilizer* is necessary for both stabilization and protection, carrying current when a (local) partial transition to the normal state occurs inside the superconducting filament. In a superconducting wire or tape for HEP magnets, the typical ratio λ of stabilizer to superconductor is in the range of 1–2. Lower values of λ are usually not feasible for reasons of protection, given the large energy stored per unit volume of conductor in accelerator and detector magnets. Larger values of λ, as could be demanded for protection, are not practical as the conductor manufacturing may become problematic, and the conductor's efficiency decreases. The stabilizer must maintain its properties through the wire and coil processing, and in particular achieve a high residual resistivity ratio (RRR), ideally combined with a low magnetoresistance. For the high-purity copper commonly used in LTSs, a good target is an RRR of about 100 or higher, which corresponds in zero magnetic field to a resistivity in the range of 1.6×10^{-10} Ω m or less. It should be noted that the RRR reduces owing to the magnetoresistance of the material, which has a substantial effect especially on high-purity materials.

2.3. *Magnetization, flux jumps, AC loss*

A magnetic field change induces shielding currents in a superconductor that do not decay. For this reason these currents are referred to as *persistent*. The magnetic moment per unit volume M associated with persistent currents is proportional to the current density of the shielding currents, J_c, and the characteristic size of the superconductor, D:

$$M \approx J_c D. \tag{3}$$

The magnetization can attain large values at low background field, where J_c is large, and when the superconductor has a large dimension exposed to the field change. In LTSs, $\mu_0 M$ at the typical injection fields of modern synchrotrons (e.g. 0.5 T for the LHC) is in the range of several tens of mT (Nb–Ti) to hundreds of mT (Nb_3Sn). Such a magnitude is sufficient to perturb the field generated by the magnet, and hence requires careful control and compensation. Furthermore, if the magnetic energy stored in the shielding currents becomes sufficiently large compared to the heat capacity of the superconductor, the magnetization can collapse suddenly in a process referred to as a *flux jump* [46]. Flux jump instabilities plagued early magnets built with monofilamentary wires and tapes, whose characteristic dimension was of the order of a millimeter. Flux jumps can be controlled by subdividing the superconductor into small filaments, which both decreases the magnetization and improves the magnetic and thermal stabilizing effect of the low-resistance matrix.

As with the bulk behavior described above, field variations induce shielding currents between

the superconducting filaments. These currents couple the filaments electromagnetically by finding a return path crossing the conductor matrix. The amount of filament coupling depends on the resistivity of the matrix, which has to be low for good protection, and the geometry of the current loop. In the extreme case of wires and tapes with untwisted filaments, coupling currents could travel along large lengths (such as the kilometer length in a magnet) and find a low cross-resistance. The net effect would be that the multifilamentary matrix would respond to field changes as a single bulk filament, losing the advantage of fine subdivision. Decoupling of the filaments is achieved by shortening the current loop, by twisting the wire with a typical pitch on the order of a few millimeters.

2.4. *Mechanical properties*

Superconducting wires in an accelerator magnet operate under large deformations as a result of the thermal contraction differences during cooldown and the high Lorentz forces that develop during charging of the magnet. The strain on the superconductor that is generated by the thermal contraction differences is predominantly longitudinal, and typically on the order of a few tenths of a percent compressive strain, since the wire matrix and the magnet construction materials mostly exhibit a larger thermal contraction than the superconducting materials. The Lorentz loads are predominantly transverse and result in operating stresses in the range of 50–100 MPa in the present accelerators, and up to projected values of 150–200 MPa for high-field magnets made of Nb_3Sn.

An obvious way to reduce the strain due to the difference of thermal contraction is to choose magnet construction materials that match the thermal contraction of the superconducting material. In practice, this is not always possible due to conflicting demands on construction materials. As to transverse loading, the stress generated by the Lorentz load depends on the current density and the thickness of the winding pack [23]. A thin winding pack with high J_{avg} makes very effective use of the superconductor, but experiences higher stress than a thicker winding pack with a lower J_{avg}. On the other hand, there are limits to the thickness of the winding given by available space, and a thick winding becomes ineffective from the point of view of the field generated, the amount of material required, and the cost. In practice, J_{avg} and winding thickness are a compromise between the effective use of the conductor, and acceptable Lorentz loads. The role of the Lorentz loads in this compromise becomes more important in high-field magnets, where the use of brittle Nb_3Sn and HTS conductors results in magnet designs that are stress-limited to the maximum acceptable by the material. Among the possible mitigation measures, the winding of Nb_3Sn high-field magnets is precompressed at room temperature and during cooldown, so that the peak field (and minimum margin) region unloads when the magnet is powered [47, 48].

Understanding the superconductor response to mechanical loads is of paramount importance, especially in the perspective of the use of superconductors for the next generation of high-field accelerator magnets. The behavior of superconductors under stress and strain is mainly determined through axial strain experiments on the wires and tapes [49–58], and through transverse pressure experiments on Rutherford cables [33, 59–65]. In the sections below we review the main results obtained to date.

2.4.1. *Axial strain sensitivity*

A summary of the typical behavior of the critical current as a function of axial strain for the various superconductors is presented in Fig. 4. The behavior of Nb–Ti under axial strain is omitted, since Nb–Ti only exhibits relevant sensitivity to axial strain above 1% [66], which is beyond the strain range that is acceptable in magnets. Nb_3Sn and YBCO both

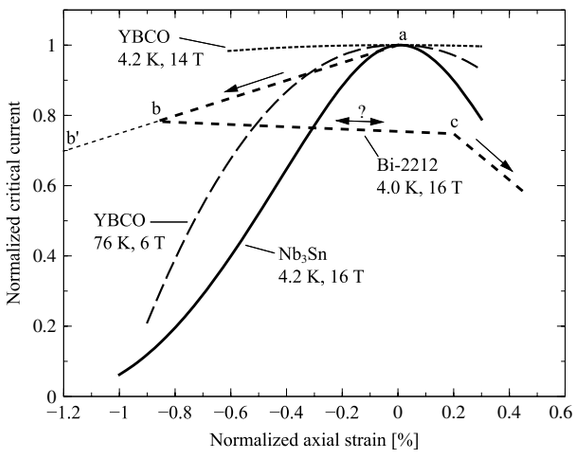

Fig. 4. Typical variations of the critical current as a function of axial strain for Nb_3Sn [49, 50], Bi-2212 [51, 52], and YBCO [55–58].

exhibit a reversible sensitivity to axial strain. Nb_3Sn can be axially compressed to beyond 1% strain, and the I_c will fully recover when the axial compressive strain is released. In axial tension, the reversibility only occurs up to the so-called irreversibility strain limit (ϵ_{irr}), beyond which cracks start to form in the Nb_3Sn volume. The magnitude of ϵ_{irr} depends on the wire layout, and appears also strongly related to the inner architecture of the strand (e.g. the filament or subelement diameter) as well as the use of dopants (e.g. Ti appears to yield a higher ϵ_{irr} than Ta). The typical (reversible) reduction in I_c in Nb_3Sn amounts to -50% at -0.5% compressive strain at 4.2 K and 16 T (Fig. 4). The sensitivity of the I_c of Nb_3Sn to axial strain, i.e. the steepness of the reduction, increases with the magnetic field and with the temperature, i.e. when approaching the field–temperature superconducting phase boundary [49].

The strain sensitivity of YBCO was initially dominated by crack formation in the YBCO layers, and it is only recently that reversible behavior has been observed [54]. The observation of reversibility in modern YBCO conductors is partly a result of improvements in measurement techniques, and likely also due to improvements in conductor fabrication, where a homogeneous YBCO layer is well bonded to a strong substrate that prevents local stress concentrations. Since YBCO was until recently mainly developed for the electric utility industry, most measurements were so far performed at liquid nitrogen temperature, and the material exhibits a sensitivity to strain at 76 K that is comparable to Nb_3Sn at 4.2 K (see Refs. 55 and 56, Fig. 4). More recent reversible data at 4.2 K and medium magnetic field [57, 58] show a striking reduction in the sensitivity to strain, perhaps due to the fact that at these magnetic fields and temperatures the material is very far away from the field–temperature superconducting phase boundary. A virtual absence of strain sensitivity over an axial strain range that is about 1% wide holds significant promise for the application of YBCO in high-field magnets.

The behavior of Bi-2212 under strain is, in contrast to Nb_3Sn and YBCO, to a large extent dominated by irreversible reductions in the critical current, which can be attributed to crack formation in the Bi-2212 [52, 67]. For many years, the behavior of the I_c of Bi-2212 under axial strain could be described according to the following model that was introduced in the mid-1990s [51]. A compressive strain, such as that introduced by the larger thermal contraction of the Ag–alloy matrix compared to the Bi-2212, causes an initial, irreversible reduction of I_c (point a to point b in Fig. 4). A further increase in the compressive strain causes a further irreversible reduction of the I_c (point b to point b'). When tensile strain is applied (point b to point c), the critical current reduces only slightly compared to the strong initial irreversible reduction, until at point c cracks appear and the I_c collapses irreversibly.

The plateau between points b and c is quasi-reversible: When the strain is cycled along this plateau, a slight initial further irreversible reduction of I_c occurs, until about 10–50 cycles, after which the I_c reduction stabilizes [68]. In more recent work [52], increased reversibility was observed, and it is suggested that the irreversibility is a result of local stress concentrations around the porosity and voids that plague the present Bi-2212 wires (see Sec. 4), and that the behavior on the plateau is in principle intrinsic and related to strain-induced changes in the field–temperature phase boundary [53], similar to Nb_3Sn [49], and as recently suggested for YBCO [55–57]. Overall, these trends hold promise for when Bi-2212 wires can eventually be made dense, which is required to increase the current density (Sec. 4), even though Bi-2212 might still be hindered by the fact that a brittle web of Bi-2212 is present in a soft matrix, and local stress concentrations will inevitably develop under load. Nevertheless, ongoing developments on round wire Bi-2212 will likely change its behavior under stress and strain. As it is, even with the present material, and accepting an initial loss of 20% of I_c, it seems that Bi-2212 can accept the strain range of 1% relevant for magnets.

2.4.2. *Transverse pressure on cables*

The superconducting cables must be capable of tolerating, reversibly, transverse stress up to 150–200 MPa, and the associated deformations, including all stresses at intermediate steps during magnet manufacturing and cryogenic operation. Such large loads are not problematic in Nb–Ti Rutherford cables, due to the limited sensitivity to strain in combination with the ductility of the alloy. However, for Nb_3Sn, with its brittleness and large sensitivity to strain,

large transverse loads can be an issue. A large number of transverse pressure experiments have been performed on Nb_3Sn Rutherford cables during the 1990s at the University of Twente in The Netherlands in an 11 T solenoid [59–62], and by Lawrence Berkeley National Laboratory, Berkeley, CA, USA (LBNL), at the National High Magnetic Field Laboratory in Tallahassee, FL, USA in an 11 T split pair magnet [63, 65]. These measurements were performed to establish the acceptable load limits for the first Nb_3Sn dipole magnets poised to surpass the 10.5 T magnetic field record of dipoles made using Nb–Ti technology [44, 69], namely Twente's 11 T MSUT magnet [70] and LBNL's 13.5 T D20 [71]. The data from the different transverse pressure systems are comparable [33], and established the 150–200 MPa load limit for Nb_3Sn accelerator magnets which is still used.

The benchmark 150–200 MPa safe limits were established from measurement on medium-current-density wires. The current density in Nb_3Sn increased by more than a factor of 2, from 2000 to 2005 (Fig. 1), and to determine whether similar transverse pressure limits were valid for modern high-current-density wires, new transverse pressure experiments were performed. The more recent measurements were performed on wires to try to establish a more economical alternative to complex and expensive full-size cable experiments. The results from transverse pressure experiments on wires [72–76], however, showed a significantly larger reduction in the critical current with transverse pressure, which triggered worries as to whether high-current Nb_3Sn Rutherford cables would be more sensitive to transverse pressure, and therefore unsuitable for very-high-field magnet designs. These results contrasted with the successful test results from magnets, which were loaded to the 150–180 MPa region [77]. It was found that the larger I_c reduction observed in single-wire experiments was due to insufficient side support, as well as the absence of epoxy impregnation in some cases, which were shown to be defining factors in earlier cable experiments [59]. The intuitive explanation is that transverse loading in one direction, such as loading a round wire between parallel plates, causes stress concentration at the contact and strong shear stresses inside the wire. Local stress concentrations and shear stresses are strongly reduced once the wire has a lateral support, as provided by the neighboring wires of a cable. In addition, the epoxy that impregnates the wire tends to redistribute the local transverse force and produce a stress state that approaches hydrostatic conditions. This has been proven recently on modern, high-J_c Nb_3Sn wires [78], confirming that the large observed degradation in single-wire measurements quoted earlier is a measurement artifact. A defining test of the US LHC Accelerator R&D Program (LARP) TQS03 magnet at CERN [79], in which the magnet was preloaded up to 260 MPa in the windings while experiencing very limited permanent degradation, re-established Nb_3Sn firmly as the conductor of choice for future upgrades of the LHC.

In contrast to the well-established data on LTS Rutherford cables under transverse loads, little is known for the HTS conductors. To the authors' knowledge, there exists only one transverse pressure experiment on Bi-2212 Rutherford cables [64], while the transverse pressure effects on YBCO Roebel cables are, so far, not documented in the available literature. The limited data on Bi-2212 Rutherford cables suggest a less favorable sensitivity to transverse pressure, and indicate irreversible damage above perhaps already 60 MPa. It should be noted that these data stem from older-generation Rutherford cables, in which the Bi-2212 has perhaps a high void fraction (see Sec. 4). Nonetheless, even at 100% dense Bi-2212, the prospect of high transverse loads on a brittle web of Bi-2212 in a soft matrix does not seem favorable, but without available data such statements are highly speculative. New characterizations of further-optimized Bi-2212 conductor, in which the Bi-2212 ideally approaches a 100% density, should determine what loads are acceptable, and to what extent internal reinforcements in the windings should be included (at the cost of current density) to intercept the accumulation of Lorentz loads.

2.5. *Manufacturing properties*

A good superconductor must be easy to manufacture and be cost-effective. An efficient manufacturing process, associated with high yield, is a prerequisite to achieving low cost. For this reason a good indicator is the piece length, which should be in the range of 1 km and longer for HEP applications. Processing after magnet winding, and material compatibility, are additional parameters to be considered in the

final cost. One such example is Nb_3Sn, which needs a high-temperature heat treatment ($>600°C$) for the formation of the superconducting phase, which is not compatible with organic insulators. Further, HEP magnets put large values on homogeneity of performance, as well as consistent production over a typical project time span, which can be of several years from inception to operation in an accelerator. Indeed, as shown by the example of the Nb–Ti production for the LHC [85], homogeneity of the critical current, stabilizer fraction, magnetization, wire geometry and mechanical properties can have a vital impact on the final performance of the magnet system.

3. State-of-the-Art Conductors for HEP

3.1. *Nb–Ti*

3.1.1. *Discovery and beginnings*

The alloy Nb–47%Ti [80] is undoubtedly the most successful practical superconductor to date. Nb–Ti rapidly followed Nb–Zr as one of the first commercial superconductors. These two alloys were mechanically very tough, as they were originally developed for high-strength rivets. Among the two, Nb–Ti is easier to manufacture, possesses superior mechanical strength, and has a 2 T advantage in the upper critical field. For these reasons Nb–Ti became the dominating conductor used in the magnets built at that time, and long after [12]. Fabrication of Nb–Ti became an industrial-grade process with the advent of the multifilamentary conductor made by Prof. R. Rose and his MIT group in 1964 [81, 82] using a process developed by F. Levi [83] and first commercially produced by Imperial Metal Industries, Ltd.

3.1.2. *State of the art*

The initial industrial productions, for example used for the construction of the Tevatron, had a specified current density J_c of $1800\,A/mm^2$ at 5 T and 4.2 K, and a filament diameter of about $10\,\mu m$, which at the time was a significant production challenge. The understanding of the physical mechanisms of pinning, and in particular the key role of high homogeneity in the initial Nb–Ti alloy in combination with advanced processing to cause a fine distribution of precipitated normal-conducting α-Ti pinning centers, led to a dramatic jump of J_c in the years 1980–1985. This performance improvement was the fruit of a number of activities within the R&D program coordinated by the SSC Central Design Group [84]. The resulting material, dubbed Hi–Ho Nb–Ti, has become the present industrial standard.

Nb–47%Ti has a critical temperature of 9.2 K, and a critical field of 14.5 T. At 4.2 K and 5 T the non-Cu critical current density J_c is approximately $3000\,A/mm^2$, while at 7.5 T and 4.2 K J_c drops to $1500\,A/mm^2$. Cooling to 1.9 K results in this point being shifted in field by 3 T, up to 10.5 T. This field range represents the upper (quench) limit for the use of Nb–Ti in accelerator dipole magnets, leading to a safe 8 T operational limit in large-scale accelerator applications. Nb–Ti is easily available in long lengths (a few km piece length) in the form of multifilamentary wires where the superconductor is dispersed in a copper matrix of high purity, with an RRR comfortably in the range of 200. A thin Nb barrier separates the Nb–Ti alloy from the copper, a heritage of initial developments that wished to avoid the formation of inter-metallics of Cu and Ti during high-temperature extrusion and annealing heat treatments.

One example of industrial wire, a double-stack LHC inner strand, is shown in Fig. 5. It contains approximately 9000 filaments of $7\,\mu m$ diameter in a matrix with an outer diameter of 1.065 mm and a Cu:Nb–Ti ratio of 1.65. Standard industrial production yields filament sizes of a few μm (5–10), which is mandatory for reducing the field perturbations induced by persistent current magnetization. A typical value of magnetization due to persistent currents is shown in Fig. 6 for an LHC Nb–Ti strand with a filament diameter of $6\,\mu m$. The magnetization at the LHC injection field, around 0.5 T, is approximately $\mu_0 M \approx 10$–$15\,mT$, which is a representative value for this product. Filaments in this range of dimensions are also stable against flux jumps, which make the behavior reproducible and easier to control. Finally, homogeneity of Nb–Ti production is excellent, at the level of a few percent for key parameters such as critical current, magnetization, wire composition, and geometry [85]. Approximately 2000 tons per year are fabricated worldwide, mainly for MRI applications. The typical cost for the HEP-grade Nb–Ti described here is in the range of around 1–2 EUR/kAm (evaluated at 5 T and 4.2 K).

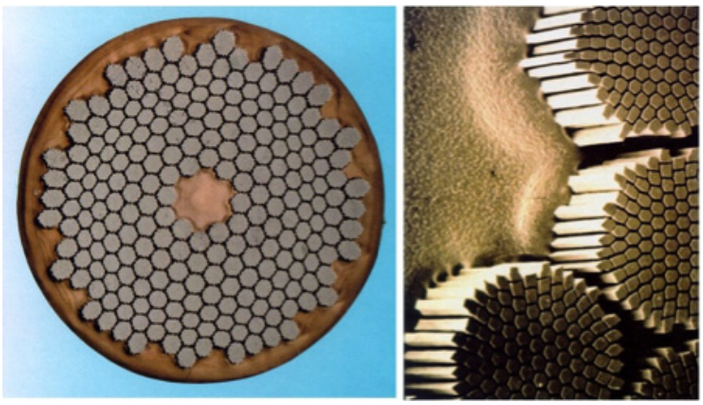

Fig. 5. One of the multifilamentary Nb–Ti strands used in the LHC. It has a diameter of approximately 1 mm, and each Nb–Ti filament (shown in the detail micrograph) has a diameter of 7 μm. The matrix is pure copper.

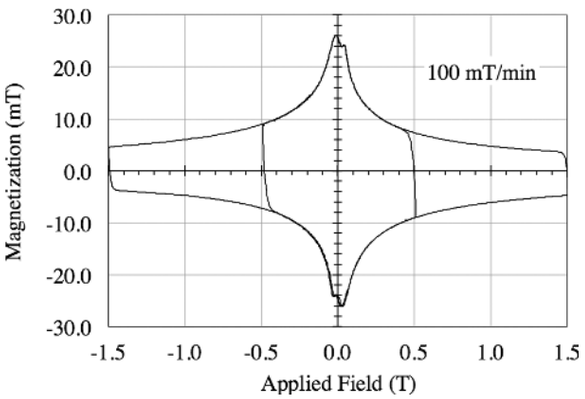

Fig. 6. Magnetization loops measured on an LHC Nb–Ti strand for the outer layer of the dipole magnets (LHC reference strand). The Nb–Ti strand has filaments of 6 μm geometric diameter. (Data courtesy of D. Richter and B. Bordini, CERN, Geneva.)

3.1.3. *Challenges*

The research on basic understanding of the mechanisms of pinning in Nb–Ti, an activity that unfolded in the late 1980s, during the years of the SSC R&D, was naturally associated with the attempt to exploit the full potential of the material in terms of critical current. The best results were obtained using artificial pinning centers (APCs) and ternary alloying with Ta. APC Nb–Ti, where the additional pinning centers are provided by a Nb or Cu structure in the Nb–Ti, has achieved critical current density in excess of 10,000 A/mm^2 at 4.2 K and 5 T [86, 87]. The APC samples are in general layered structures, fabricated by sputtering and photolithography, i.e. a process that provides highly anisotropic properties, and far from industrial practice. The addition of Ta in the range of 15–25% produces a ternary alloy that has a critical field increased by approximately 1 T, at the loss of some of the α-Ti-precipitate pinning centers [84]. These R&D results show that there may still be room for improvement. None has become an industrial standard, however — possibly influenced by the much greater potential of Nb_3Sn.

A second field of active research is the application of Nb–Ti to fast-cycled accelerator magnets [88]. This is a relatively old target, already pursued in the mid-1970s when superconducting cycled magnets were developed at Rutherford Laboratory [89], CEA, and the Kernforschungszentrum Karlsruhe [90]. Among the prospective applications at the time was a superconducting option for the CERN Super Proton Synchrotron (SPS) [91], then built using resistive magnets. The main focus of research at the time was on how to reduce the ac loss associated with field sweeps in the superconducting filaments (hysteresis loss), as well as in the wires and cables (coupling loss) on cycled magnets, and this work boosted the understanding of the role and means of twisting and transposition.

The development of low-loss Nb–Ti strands with ultrafine filaments (0.1 μm) and highly resistive barriers (Cu–Ni) received a great impulse in the following years as part of the R&D on electrical machines and ac applications at 50/60 Hz [92]. This program was abandoned given the weak economic case, but some of the results were exploited in the construction of a low-loss Nb–Ti conductor used to wind a demonstration poloidal coil [93] for high-voltage

pulsed operation in the Tore Supra tokamak. More recently, given the success of the slowly ramped synchrotron quoted earlier, low-loss Nb–Ti strands and cable are receiving renewed interest for fast-cycled machines such as the SIS-100 and SIS-300 accelerators which are part of the FAIR complex, under construction at GSI [94]. The main argument for the use of superconducting magnets in this case is the installed electrical power and the cost of energy, which translates into the need to minimize the ac loss caused by the magnetic field cycle.

To reduce the ac loss, it is necessary to:

- Reduce the size of the filaments, which decreases the magnetization and the hysteresis loss;
- Use small-diameter strands, with a tight twist pitch, which reduces the voltage driving coupling currents across the interfilamentary matrix;
- Use resistive matrices or resistive barriers within the stabilizer matrix, to increase the resistance of the path of coupling currents.

In the range of wire diameters of interest, 0.5–1 mm, Nb–Ti filaments of 1–2 μm seem to be a practical lower limit. The fabrication of such assemblies becomes challenging and, with on the order of 100,000 filaments in the cross-section, single stacks are no longer feasible. A double stack of subelements can be effective, but the inhomogeneities among the materials can result in severe deformation of the fine filaments, causing loss of J_c, and a filament size that is larger than the ideal one. Furthermore, fine and closely spaced filaments tend to couple with each other, either through direct contact or because of electrical proximity. The resulting magnetization is larger than that expected from the single-filament geometry, as if it were produced by an *effective* filament of increased diameter. This effect, measured in Cu/Nb–Ti strands with filaments below 4 μm, can be mitigated by adding small percentages of magnetic materials such as Ni or Mn in the stabilizer matrix. Unfortunately, magnetic materials have an adverse effect on J_c, and in general fine filament wires fall short of the high J_c standard quoted earlier.

The interplay of filament diameter and critical current density can be seen in Fig. 7, which shows a scatter plot of hysteresis loss for a ± 1.5 T bipolar cycle, proportional to the magnetization, and critical current density at 4.2 K, 5 T for a selection of

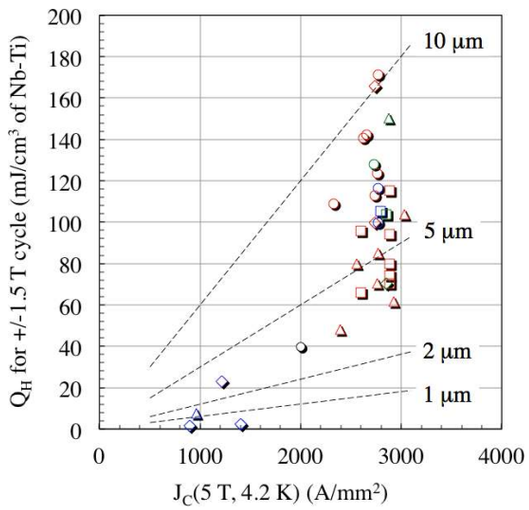

Fig. 7. Scatter plot of hysteresis loss per unit superconductor volume for a bipolar ± 1.5 T cycle at 4.2 K versus J_c at 4.2 K and 5 T of the same wire, for a selected number of standard and low-loss wires produced in the past 15 years. The lines represent computed loss using a fully penetrated filament model, and filament diameters of 1, 2, 5, and 10 μm.

standard (LHC, ITER) and R&D Nb–Ti strands produced in the past 15 years. The plot also contains lines of hysteresis loss at constant filament diameter, and shows that high J_c can be achieved with an effective filament diameter down to about 3 μm. Smaller values of the filament diameter are feasible, but this seems difficult to achieve without a significant loss of J_c.

The use of resistive matrices is of special importance for reducing the coupling loss due to currents that tend to shield the interior of a strand by flowing in the superconducting filaments at the strand surface, and closing through the stabilizer. It is not possible to increase at will the electrical resistivity of the matrix, as low resistivity is required for stabilization and protection. An alternative is to introduce resistive barriers in the cross-section, thus decreasing detrimental transverse conductivity while maintaining beneficial longitudinal conductivity. This is done by introducing materials such as Cu–Ni as a spacer among filaments, subelements, and around the multifilamentary region. Using such resistive barriers, the time constant of the strand coupling currents can be reduced from the order of magnitude of tens of ms (e.g. 25 ms for an LHC inner layer strand) to below 1 ms, with a proportional reduction of ac loss.

3.2. Nb_3Sn

3.2.1. *Discovery and beginnings*

The intermetallic compound Nb_3Sn [95] is the second LTS material that has found its way from material research to large-scale applications. Nb_3Sn is a brittle compound, and all modern manufacturing routes involve assembly of the precursor elements Nb, Sn and Cu additions (necessary for reducing the temperature at which Nb_3Sn is formed; see Ref. 96 and later discussion) into large-size billets that are extruded and/or drawn to the final diameter wire. The Nb_3Sn is then formed by a solid state diffusion reaction that is induced by a heat treatment at high temperature. Various manufacturing routes have been established industrially, resulting in wires with different critical current density and filament size.

As reported earlier, the initial manufacture of technical Nb_3Sn was achieved by filling Nb tubes with crushed powders of Nb and Sn. The tube was sealed, compacted, and drawn to long wires. This primitive Powder-in-Tube (PIT) technique required reaction at high temperature, in the range of 1000–1400°C, to form the superconducting phase. The high temperature, which causes excessive grain growth and low vortex pinning, is required as a result of the presence of two very-low-T_c Sn-rich line compounds ($NbSn_2$ and Nb_6Sn_5) that are stable in the binary compound below approximately 930°C [97]. An early alternative to the PIT was the fabrication in the form of tapes, by passing a Nb tape through a bath of molten Sn, and reacting the coated tape to form Nb_3Sn [98]. Although successful in demonstrating the use of Nb_3Sn in high-field magnets, neither technique was practical. The large filaments in the case of the PIT wire, and the inherently large aspect ratio of the tape, invariably result in large trapped magnetization and flux jump instabilities.

In the late 1960s, Tachikawa introduced an alternative concept based on solid state diffusion. In his original work on V_3Ga (another superconducting intermetallic of the same family of materials with the A15 crystal structure), he used small filaments of V surrounded by a Cu matrix alloyed with Ga [99]. Solid state diffusion at high temperature mobilizes one of the two components (Ga), which reaches the filament (V) and reacts to form the superconducting phase. The same principle has been exploited to fabricate Nb_3Sn wires by the so-called bronze route, which is today one of the leading techniques for manufacturing Nb_3Sn.

3.2.2. *State of the art*

Industrial Nb_3Sn is presently produced by one of the following three manufacturing techniques: bronze route, internal tin, and PIT (see the architecture schematics shown in Fig. 8).

A bronze route wire is made up of a large number of Nb or Nb-alloy filaments assembled in a Sn-rich bronze matrix. The composite is usually inserted in a can of high-purity copper stabilizer, with a thin barrier of material chemically inert to Cu, such as Nb, Ta, or Va. The assembly is then extruded and drawn to the final wire diameter. The superconducting phase is formed by submitting the wire to a heat treatment at a temperature in the range of 600–700°C, i.e. significantly lower than the temperature required for the formation of Nb_3Sn from a binary mixture of Nb and Sn. This is enabled by the fact that the presence of Cu destabilizes the Sn-rich line compounds [96, 97]. The lower temperature prevents the excessive grain growth that is inevitable in binary systems, thereby increasing the pinning efficiency. At sufficiently high temperature, Sn diffuses in the Cu–Sn matrix and reacts with the Nb filaments to form the superconducting Nb_3Sn phase.

The bronze route is a very-well-established process, which is used at present to produce most industrial Nb_3Sn. The main drawback of the bronze route comes from the limit of Sn solubility of 9.1 at.% (or 15.8 wt.%) in the ductile α-bronze. In fact, not all the Sn content in the bronze can be mobilized for reaction with the Nb filaments, and the Sn-depleted bronze matrix left after heat treatment takes a significant portion of the total non-Cu cross-section of the wire. Although beneficial for keeping the superconducting filaments physically decoupled, the matrix detracts from the real estate available in the wire for the superconducting phase. The limited Sn source further results in the formation of a relatively large fraction of off-stoichiometric niobium–tin [101] (which is stable from 18 to 25 at.% Sn [97]) with a reduced field–temperature phase boundary [102] that is not superconducting at higher magnetic fields. The relatively small fraction of Sn-rich Nb_3Sn, combined with the lost real estate that is occupied by the bronze, results in an upper limit to the

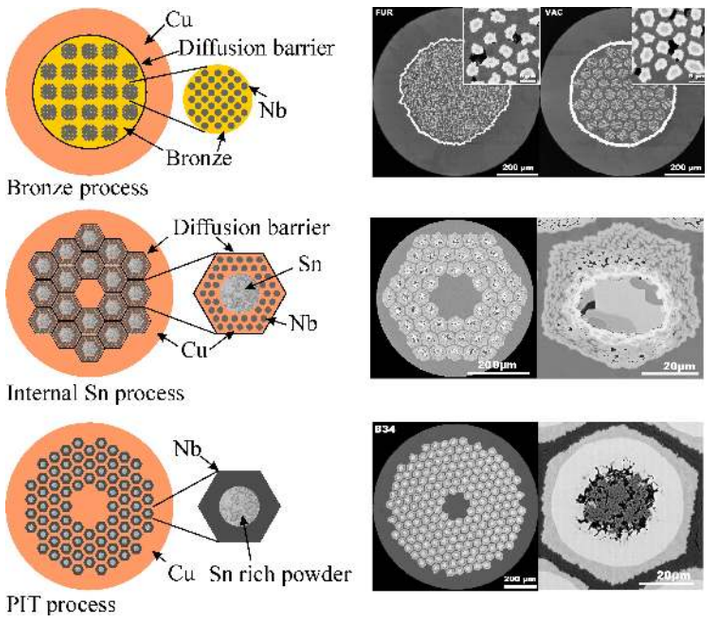

Fig. 8. Schematic overview of Nb_3Sn wire manufacturing processes, reproduced from Ref. 39 and based on Ref. 100. The schematic arrangement of materials and subelements is only for illustration purposes.

non-Cu critical current density J_c in the range of $1000\,A/mm^2$ at 4.2 K and 12 T in optimized wires.

An alternative to the bronze route wire consists in assembling a large number of Nb or Nb-alloy filaments and pure Sn or Sn-alloy rods in a Cu matrix. Such an assembly can be surrounded by a barrier that prevents diffusion of Sn, and further enclosed in a high-purity copper can. The stacked assembly is drawn to the final size of the wire. Restacking of assemblies is commonly done to decrease the final size of the subelements. Upon heat treatment, a cross diffusion process between Sn and the Cu matrix takes place, resulting in a Sn flow toward the multifilamentary region and subsequent reaction of Nb and Sn into Nb_3Sn. Several variants of this process have been devised, differing mainly in the way the various initial components are arranged. Because of the presence of the Sn source internal to the assembly, they are generally referred to as internal tin techniques.

By comparison with the bronze route, an internal tin wire avoids the limitation on the amount of Sn inherent to its solubility in bronze, and increases the freedom in the layout. High non-Cu critical current is achieved by maximizing the amount of Nb in the matrix, keeping the Cu matrix fraction to a minimum, and introducing the quantity of Sn required for complete reaction to close to stoichiometry. This apparently trivial task is in reality a tantalizing balance of cross-section optimization, diffusion and reaction kinetics, and practical manufacturing issues.

The optimization of the internal tin technique, fostered by the US DOE Conductor Development Program (CDP), launched in 1999, produced the spectacular jump in J_c visible in Fig. 1. One of the most successful high-J_c internal tin processes developed within the scope of the CDP is the Restacked Rod Process (RRP®) of Oxford Superconducting Technology, which regularly achieves non-Cu J_c values in excess of $3000\,A/mm^2$ at 4.2 K and 12 T. To reach such high values of J_c, both the quantity (the amount of superconductor that is formed in the non-Cu fraction) and the quality (grain refinement, Sn content, and ternary element addition) of the Nb_3Sn must be optimized. This is possible by reducing the fraction of Cu in the matrix — also referred to as the local area ratio (LAR) — to a practical manufacturing minimum in the range of 0.1–0.3, introducing alloying additions such as Ta or Ti, and by an optimized heat treatment schedule. Furthermore, the barrier that separates the multifilamentary region from the high-purity Cu is made of Nb and partially reacted during heat treatment, thus adding to the final superconducting cross-section. After heat treatment, the tightly packed

Nb filaments and the reacted portion of the barrier grow into a completely connected cross-section of Nb_3Sn, fully coupled, whose characteristic dimension is hence approximately the size of the stacked subelement, which can be relatively large (50–100 μm).

Finally, high-J_c Nb_3Sn wires can be manufactured using an evolution of the PIT process originally devised by Kunzler. The idea developed in the mid-1970s at the Netherlands Energy Research Foundation (ECN) consisted in stacking tubes of Nb, filled with crushed powders of $NbSn_2$ and a small percentage of Cu additive (necessary for the destabilization of the Sn-rich line compounds), in a high-purity Cu matrix. The stacked assembly is drawn or extruded to the final diameter and heat-treated, where attention should be paid to preventing the reaction front reaching the outer boundary of the Nb tube. Initial PIT wires produced by ECN, with 18–36 tubes in the Cu matrix, achieved a non-Cu J_c of about 500 A/mm^2 at 4.2 K and 12 T. These values were consistently improved in the 1980s, until the 1990s production wire with 192 tubes reached a non-Cu J_c of 1700 A/mm^2 at 4.2 K and 12 T. Further optimization of the layout, powders, the use of Ta as the alloying element in the Nb tube, and industrialization took place in the 1990s and 2000s, first at ShapeMetal Innovation (SMI) in Enschede, The Netherlands, then at European Advanced Superconductors in Hanau, Germany, presently Bruker-EAS (see also Ref. 103). Industrial PIT wires from Bruker regularly achieve non-Cu J_c in excess of 2500 A/mm^2 at 4.2 K and 12 T.

In practice, the OST RRP and Bruker PIT are at present the only two options of Nb_3Sn with sufficiently high J_c for HEP applications, and available in large quantities from industry. In Fig. 9 we show a cross-section of two standard layouts: a 0.7 mm RRP 108/127 stack and a 1 mm 192-tube PIT. Figure 10 shows typical critical current values of two such strands, heat-treated using the recommended schedule from the manufacturer.

It is to be noted that the difference in J_c of the two processes, which is significant at 12 T, tends to decrease above 15 T and the two curves cross around 20 T. The current-carrying capability at medium (i.e. 12–15 T) versus high field (i.e. 20 T and higher) can be manipulated in various ways. The upper critical field (H_{c2}) (and to a lesser degree the critical temperature T_c) can be increased by varying the amounts of alloying elements such as Ta or Ti [104], which will increase specifically the high-field performance. The upper critical field maximizes for 1.5 at.% Ti and for 4 at.% Ta addition. The difference is due to the fact that Ta replaces Nb and Ti replaces Sn in the Nb_3Sn lattice (suggested in Ref. 105 and confirmed by Ref. 106). Commercial Nb–7.5 wt.%–Ta alloy, for which the Ta content cannot be readily varied, is used in most RRP and PIT wires, and H_{c2} cannot be varied by changing the Ta content. Recent RRP wires combine pure Nb rods with commercially available Nb–47 wt.%–Ti rods, and can vary the amount of Ti by varying the ratio between the Nb and Nb-alloy rods, and therefore manipulate H_{c2} through compositional variations.

A second way by which the J_c at medium fields can be balanced against high-field performance is through the reaction temperature. More aggressive reactions at higher temperature increase the Sn activity, and therefore generate a Sn-richer Nb_3Sn with a higher H_{c2} [97, 102], and thus increased performance at higher field. This goes, however, at the cost of pinning efficiency, since the grain dimension of the reacted Nb_3Sn is a power function of the reaction temperature [103], which reduces the pinning

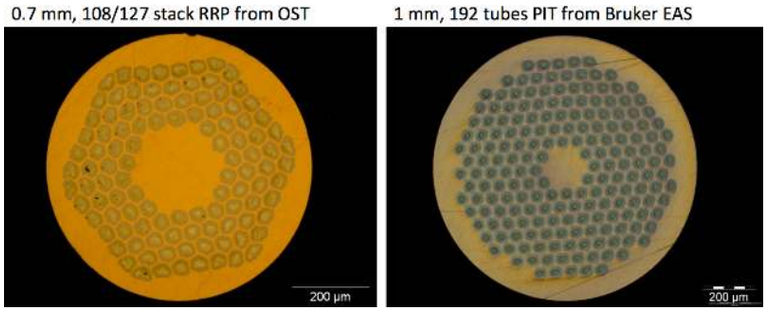

Fig. 9. Layouts from leading manufacturers of Nb_3Sn strands for HEP applications.

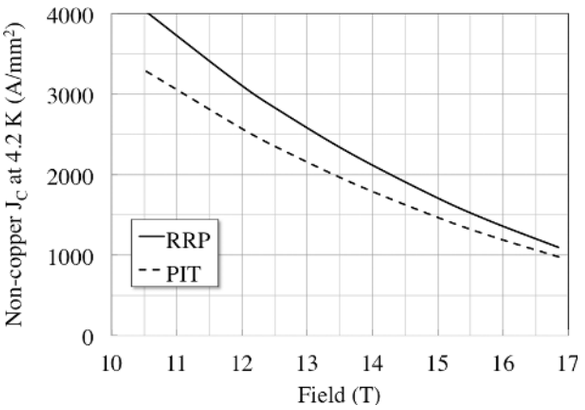

Fig. 10. Typical non-Cu J_c for the strands in Fig. 9, based on measurements at 4.2 K.

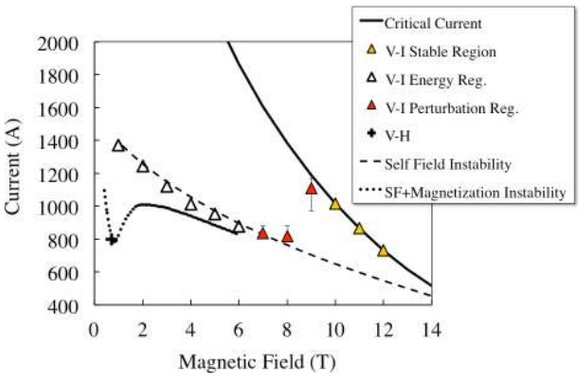

Fig. 11. Critical current and quench values as a function of the magnetic field, depicting high-field J_c values, and low- and medium-field quench values that are due to instabilities and measured using field sweeps at constant current.

force [97], and therefore the performance at medium fields. Lower-temperature reaction results in Nb_3Sn that is less rich in Sn, with reduced H_{c2} and high-field performance, but can retain smaller grains and thus increased pinning and performance at medium magnetic fields. The conductors can hence be optimized for medium- or high-field performance, and the difference between the RRP wire and the PIT wire in Fig. 10, as well as the cross-over at higher field, can be attributed to such optimizations.

3.2.3. *Challenges*

The spectacular increase of J_c achieved over the past 10 years is a great success, but has also brought a number of riddles. In some cases, magnet performance was found to be below expectations, affected by instabilities that could be reproduced in single strands and cables both experimentally and theoretically [107, 108]. The basic explanation lies in the combination of the well-known effect of flux jumps at low field, and a newly defined self-field instability at high field [109]. The performance limits are shown schematically in Fig. 11, which reports measured critical and quench currents of a 0.8 mm wire fabricated by the OST RRP process, consisting of a stack of 54 subelements of 80 μm diameter in a Cu matrix with an RRR of 80.

The upper line in the graph is the critical current I_c as obtained by measurements at high field, and extrapolated to low field. What is observed experimentally (symbols in Fig. 11) is that the wire reaches I_c at high field (above 10 T in Fig. 11). At low and medium field the wire has sudden resistive transitions well before reaching the critical current. This can be interpreted by an instability induced by the dissipation of the energy stored in the magnetization associated with the distribution of persistent current in the filaments (magnetization flux jump instability) or with the distribution of transport current among filaments (self-field instability). The magnetization flux jump instability dominates the behavior at very low field (up to 2 T in Fig. 11), and is usually evidenced by sweeping the field at constant current, a so-called $V(H)$ measurement. The severity of the flux jump instability depends on the size of the superconducting filaments. The maximum current that the wire can reach in this regime usually dips at field ranges of the order of the penetration field, when the magnetization also reaches its maximum.

At intermediate field (the range of 2–10 T in Fig. 11), the dominating effect is caused by the potential collapse of the self-field magnetization associated with the current distribution in the wire, which is usually concentrated in the external skin of superconducting filaments. The self-field magnetization is proportional to the size of the multifilamentary region in the wire. The collapse is triggered by a small perturbation that can have external origins, e.g. mechanical energy release. At moderate field (up to 8 T in Fig. 11), where J_c and the magnetic moment associated with the current distribution are large, the perturbation that is required to trigger the instability is small (the so-called energy regime in Fig. 11). At increasing field J_c decreases, the self-field magnetization also decreases, and the magnitude of the perturbation that triggers the instability increases.

This is visible in Fig. 11 as a transition region — the perturbation region from 8 T to 10 T. Eventually, the self-field instability is no longer triggered by the energy spectrum associated with the specific operating environment, and the wire reaches the critical current (above 10 T in Fig. 11).

In practice, a very high J_c, in the range of 3000 A/mm^2, is accessible only in strands of modest diameter (typically 1 mm and smaller) if the filament diameter is small (typically below 50 μm) and the RRR is large (typically above 100). Achieving simultaneously a high J_c with small filaments and high RRR is challenging for any of the leading wire manufacturing routes. The reason is that to achieve a high J_c, the filament cross-section must be reacted almost completely, with the risk of a Sn leak in the stabilizer matrix and a catastrophic drop of RRR. This is particularly true in Rutherford cables, in which the diffusion barrier is significantly distorted at the edges of the cable. In practice, a fixed thickness of the Nb barrier is left unreacted (a few μm), which is essentially a lost percentage of the filament cross-section. A demand for high RRR hence limits the maximum achievable J_c. Reducing the filament diameter while maintaining the thickness of the unreacted barrier also reduces the real estate available for reaction, and causes a reduction of the final J_c. In summary, the critical current density J_c, effective filament diameter, and RRR have a simple but very delicate interplay, which requires a careful compromise in the strand design.

The values of J_c reported earlier have been achieved with RRP and PIT wires of 50 μm subelement diameter or larger, and have resulted in RRR values in the range of 50–250, with a better average for the PIT wire at the cost of a reduced J_c. Such filaments are sufficiently small to avoid low-field instabilities, but still result in large magnetization and partial flux jumps. It is for this reason that present R&D is mostly focused on a reduction of the magnetization through assemblies of higher subelement count. The absolute value of magnetization, and the effect of the reduction of the subelement dimension, can be appreciated through Fig. 12, where we compare measurements of RRP 0.8 mm wire with a 54/61 stack (70 μm subelement), and 0.7 mm wire with a 108/127 stack (40 μm subelement), to results obtained on PIT 0.7 mm wire

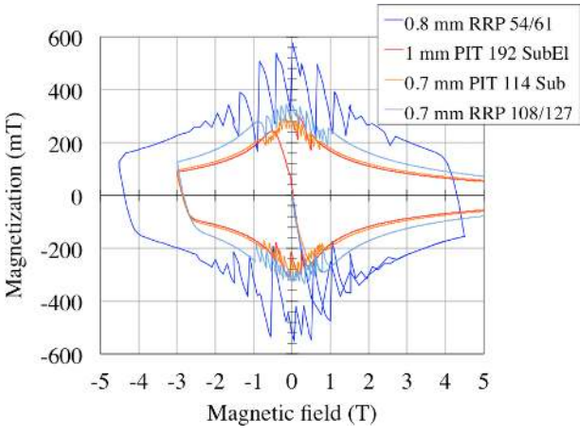

Fig. 12. Magnetization of Nb_3Sn wires of different architecture, external, and subelement diameter. (Data courtesy of B. Bordini and D. Richter, CERN, Geneva.)

with 114 tubes (45 μm subelement), and PIT 1 mm wire with 192 tubes (50 μm subelement). We observe the expected reduction of magnetization and instability in RRP wires from 70 μm to 40 μm. In addition, the fact that PIT wires have a lower J_c at low field when compared to RRP gives an additional benefit to the PIT. At comparable, or even slightly larger subelement, the low-field magnetization, and flux jumps are further suppressed.

The compromise among the demands for high J_c, high RRR, and small subelement diameter can be combined in a target performance specification for large-scale HEP applications reported in Fig. 13. The targets given there are based on data available on stability current, magnetization, and estimates for flux jump onset, and refer to strands with a diameter of 1 mm and smaller. At this diameter, an RRR of

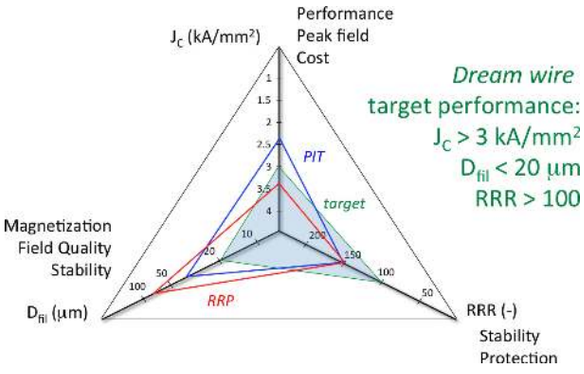

Fig. 13. Performance target space for HEP Nb_3Sn.

100 is considered sufficient to avoid significant degradation due to self-field instability. A subelement of 20 μm would lead to a magnetization width at 1 T (a sensible projected injection field) of approximately 150 mT, which is still a few times larger than that obtained in the accelerator superconducting magnets built with Nb–Ti, but within a reasonable correction range. Most important, with a subelement of this size we would expect no flux jumps at any operating temperature, including 1.9 K.

We report in the same schematic three-axis representation present typical values for the RRP and PIT technologies, which show how the subelement diameter is indeed the most challenging among the three parameters. For this reason, present R&D is mostly devoted to reducing the subelement diameter, while still preserving J_c and RRR. Specifically, OST is developing an RRP assembly of 217 subelements which has already been tested in prototype lengths and yielded promising results [110]. Similarly, Bruker-EAS is working on PIT R&D material made with 192 tubes, drawn to small diameters. Measurements of short lengths of this PIT wire drawn to 0.6–0.7 mm have recently shown that the critical current density can be preserved at marginal RRR loss, and that the magnetization exhibits no flux jumps at 4.2 K [111].

The R&D mentioned above will lead to similar subelement diameters for both routes, in the range of 30–35 μm. A further reduction to 20 μm would require assemblies of 500 subelements, which is a large number for the precise and clean conditions required for successful area reduction. Further advances will hence depend on novel fabrication technologies, as for example fostered by the US Small Business Innovation Research (SBIR) program in the US.

Finally, and most important, Nb_3Sn for HEP is at present still an expensive superconductor. With a price in the range of 10 EUR/kAm (evaluated at 12 T and 4.2 K), additional effort to reduce the price is mandatory in order to make a large-scale accelerator application a viable option. This depends, among other things, on the material yield and the capability to manufacture long piece length, in the range of several kilometers. Present production of HEP-grade material is limited — an estimate of 2 tons per year, a small quantity when compared to the ITER Nb_3Sn production, averaging 100 tons per year over the past four years. This gives confidence that production capacity will not be an issue, and a scale effect could be expected once the demand increases for the first accelerator applications.

4. Advances in HTS Materials

The maximum field that can be attained using Nb–Ti and Nb_3Sn is intrinsically limited by the field–temperature superconducting phase boundary. In Nb–Ti, $\mu_0 H_{c2}(0)$ amounts to 14.5 T, whereas for Nb_3Sn, $\mu_0 H_{c2}(0)$ has a maximum of 30 T in wires [102]. The above values must be reduced because of the need for a significant J_c and operating margin. In dipoles, Nb–Ti reaches a maximum of 80% of its H_{c2} (1.9 K), whereas Nb_3Sn reaches 65% of its H_{c2} (4.2 K) [112]. The lower percentage for Nb_3Sn is a result of the fact that the grains are approximately a factor of 10 too large to achieve optimal pinning at high magnetic fields [33].

In contrast, the upper critical field of HTSs at low temperature (e.g. 4.2 K) is 100 T or higher. As such, HTS materials, and specifically YBCO and Bi-2212, do not have an intrinsic limitation in terms of the achievable magnetic field, but they are rather limited by the stress that would be produced in the winding. This is why YBCO and Bi-2212 are presently receiving much attention from the high-field community. In the following subsections, we will report on the state of the art of these two materials.

4.1. *Bi-2212*

The main attractiveness of Bi-2212, besides the high-field properties recalled above, is that it is available as a round wire, and can thus be formed into a Rutherford cable, as has been consistently demonstrated since the 1990s [113–116]. The record J_E is around 500 A/mm^2 at 20 T, 4.2 K in a 1-m-long round wire [117] (Fig. 2), and the present long-length performance is around 200–250 A/mm^2 at 20 T, 4.2 K, and thus a factor of 3–4 too low for effective magnet windings (see Subsec. 2.1). Bi-2212 requires, as with Nb_3Sn, a so-called wind-and-react magnet fabrication process, as a result of the brittleness of the Bi-2212 in combination with the small bending radii that will be required in insert coils for hybrid Nb_3Sn/Bi-2212 magnets. Bi-2212 has to be reacted in a 1 atmosphere oxygen pressure environment around 890°C, with an accuracy of ± 1°C,

which places stringent requirements on the construction and insulation materials, as well as on the furnace control. Nonetheless, small solenoid demonstration coils have been fabricated and successfully tested at various institutes [118–120], demonstrating that the use of Bi-2212 for high-field magnets is indeed feasible.

A recent breakthrough within the US Very High Field Superconducting Magnet Collaboration (VHFSMC) [37], which focused on determining the feasibility of Bi-2212 for very-high-field magnet applications, highlighted the main current-blocking mechanism in round wire Bi-2212. It was long thought that the grain boundaries, and the formation of undesired phases, were the main current-blocking mechanisms, but it was recently pointed out that large voids, dubbed "bubbles," form inside the Bi-2212 fractions and block the current [121]. These bubbles form for two reasons. First, a residual void fraction of about 25% is required inside the Bi-2212 in wires, to allow wire drawing of the hard Bi-2212 particles inside the soft Ag matrix. This distributed void fraction agglomerates into bubbles during the partial melt reaction. Second, the bubble formation is amplified by the sudden release of oxygen from the powder during the melting of the Bi-2212, and the reaction of oxygen with contaminants, such as carbon and hydrogen, to form CO_2 and H_2O. It is assumed that pure oxygen can quickly diffuse through the Ag matrix, but the CO_2 and H_2O cannot, causing internal pressure in the wires that amplifies the bubbles. The internal pressure can even cause rupture of the soft Ag-alloy matrix that is close to its melting point, with leakage of the core constituents as a result. The Bi-2212 Strand and Cable Collaboration (BSCCo) [122] in the US, which is a continuation of the VHFSMC is, in close collaboration with industry, trying to mitigate the formation of bubbles through densification, and removal of the contaminants. Bi-2212 densification studies have increased the J_E in short wire lengths to beyond the record levels, thereby approaching the 600–800 A/mm^2 range that is needed for successful application in high-field magnets [118, 123]. Densification could, by removal of the local stress concentrations due to the presence of voids, also positively alter the behavior of Bi-2212 under mechanical loads (see Subsec. 2.4). Overall, the progress in Bi-2212 wire and magnet technology has been substantial over the last decade, and Bi-2212 appears promising once the formation of bubbles can be mitigated in long lengths of conductor.

4.2. *YBCO*

YBCO is available as a tape for which the J_c strongly depends on the direction of the applied field (Fig. 2), and it requires near-perfect texture to achieve a high J_c. The J_c anisotropy is a result of an anisotropy in H_{c2}, in combination with a reduced pinning efficiency for magnetic fields that are perpendicular to the tape face, or $H \parallel c$. The upper critical magnetic field for fields perpendicular to the tape face $\mu_0 H_{c2}(0) \parallel c \approx 120$ T, whereas $\mu_0 H_{c2}(0) \perp c \approx 250$ T [124–127].

The introduction of, for example, self-assembled $BaZrO_3$ into the YBCO layer [128] results in a nanoscale distribution of so-called BZO nanodots and nanorods that form pinning centers, specifically for field applied in the c direction, i.e. perpendicular to the tape width. This increases the J_c for this field direction, but has, so far, mainly been successful for higher temperatures [129], although the BZO does increase the overall pinning efficiency at 4.2 K [130]. The different efficiency at lower temperatures stems from the fact that the coherence length, and therefore the diameter of the flux lines, which is twice the coherence length, reduces at lower temperatures and results, in combination with reduced thermal activation of the flux lines, in different pinning interactions to dominate at 4.2 K compared to 77 K [129, 131]. As a consequence of the J_c anisotropy and the inevitable magnetic field components that are parallel to the c axis in magnets, it is, for now, more realistic to observe the current-carrying capacity in the "bad" field direction, i.e. with the field perpendicular to the broad side of the tapes.

The current-carrying capacity of YBCO with the magnetic field applied in the c direction is on the order of 400 A/mm^2 at 20 T and 4.2 K (Fig. 2). This is approaching the required current density levels, specifically since only 1% of the cross-section carries all the superconducting current. Increasing the J_E by increasing the YBCO layer thickness is difficult, since misalignment becomes more significant when the layer thickness is increased, but recent efforts to increase the layer thickness to 2 μm have been successful, and the current densities in the required 600–800 A/mm^2 levels are within commercial reach [132].

A second route to gain J_E is to reduce the substrate thickness, which now constitutes roughly 50% of the cross-section, but this means a substantial change in the delicate optimizations for the fabrication processes. Nevertheless, with presently only 1% of the cross-section being superconductor, it is clear that, as with Bi-2212, the potential of YBCO is significant.

A major obstacle to the application of YBCO in HEP magnets is that it is difficult to form a transposed cable that enables currents in the tens-of-kA region. Roebel-type cables are considered [133–135], but are still in their relative infancy. Recent tests at CERN on two Roebel cables made by Karlsruhe Institute of Technology (KIT) and General Cable Superconductors (GCS), assembled from 10 and 15 12-mm-wide tapes respectively, showed critical current at 4.2 K in excess of 10 kA in a parallel 10 T background field, and approximately 4 kA in a 10 T perpendicular field [136]. The critical current of both cables is in agreement with the value expected from single tapes, once the contributions of background and self-field are properly taken into account. With the quoted performance, these Roebel cables approach the desired target for a high-field insert, and are hence promising alternatives to Bi-2212 Rutherford cables. Many issues are still open, such as insulation, winding quality, and the mechanics of the relatively loose assembly of tapes. Recently proposed alternatives [137] provide a higher mechanical stability, but so far do not retain sufficient overall current density.

4.3. *Further challenges*

Beyond the quest for higher J_c, and the difficulty of making high-current and compact cables discussed above, Bi-2212 and YBCO share a number of common challenges. The first is the management of mechanical and thermal stresses, with acceptable and reversible critical current degradation (see also our earlier discussion). This will require fundamental work on understanding and improving the strain sensitivity of Bi-2212, and most likely the choice of a magnet design with features that limit the strain and stress in the high-field, HTS-based portion.

Material compatibility with structural alloys and insulation fibers is another matter of concern, especially for Bi-2212, which requires a high-temperature heat reaction in an oxygen atmosphere. YBCO, although not requiring a heat treatment, has been found to suffer irreversible degradation and delamination, most likely caused by differential thermal contraction with respect to impregnation resins.

Quench detection and protection is the next concern for HTS materials. At high temperatures, such as 77 K, the temperature margin is in principle sufficiently low to cause a fast normal zone propagation (NZP). On the other hand, the operating current at these high temperatures is low, and the NZP is severely hindered by the lack of driving force (I^2R) and by the large heat capacity of the materials. At low temperatures, by contrast, the heat capacity is low, and with a large J_c the operating current, and Joule heating, can be high enough to increase the NZP. On the other hand, the large temperature margin tends to slow the NZP.

Another aspect that should be considered is that for quench propagation the relevant quantity is not $H_{c2}(T)$, but rather the irreversibility field $H_{\rm irr}(T)$, at which the flux lines become depinned. For round wire Bi-2212 the irreversibility line is low, and crosses 20 K at 10 T [127], therefore reducing the temperature margin for high-magnetic-field applications at 4.2 K to levels that are comparable to those of Nb_3Sn. This suggests that with an appropriate choice of the superconductor operating point and sufficient current density to drive the NZP, the NZP velocities might become high enough to allow the detection of quenches in magnet systems. In this respect, the fact that HTS will mainly be used as the high-field insert of a background magnet will be beneficial. Note, however, that for YBCO, a similar appreciable lowering of the temperature margin with an increasing magnetic field is not observed, as a result of a much higher $H_{\rm irr}(T)$ [127].

Recent experiments on small-scale coils built with Bi-2212 and operated at 40–80% of I_c up to 20 T have shown an NZP as small as a few cm/s [138], conflicting with the promise of a low irreversibility line. For now, at least in small Bi-2212 coils, voltage–current transitions can be readily measured [116], rendering the requirement of a high NZP for quench detection less urgent, but this might change once conductors become more homogeneous and the coils larger.

The above discussion leads to the conclusion that it is not clear at forehand whether quench detection and protection will be a major issue for high-field HTS magnets, but the limited data available on

high-field NZP seems to suggest that the situation is unfavorable. A wider experimental database and improved understanding is definitely a high priority.

YBCO and Bi-2212 have in common the fact that they do not have well-separated, transposed filaments. This results in large magnetic moments that are detrimental to the field quality of an accelerator magnet. Secondary to the issues above, but mandatory for an application to the high accuracy of an accelerator magnet, the matter of filament diameter and control of coupling will have to be addressed in HTS wires, tapes, and cables.

Finally, with a cost in the range of 200–400 EUR/kAm (evaluated at 20 T and 4.2 K), there is clearly a large optimization work required on the production chain before HTS materials can be used on a large scale.

5. Superconducting Cables

Wires and tapes manufactured with the LTS and HTS materials listed above carry currents in the range of a few hundred amperes, and are appropriate for winding small magnets, where the magnet inductance and stored energy are not an issue. On the other hand, the large-scale dipole and quadrupole magnets of an accelerator are connected in kilometer-long strings, and the stored energy can reach hundreds of MJ, up to the 1 GJ of an LHC dipole sector powered at nominal current. To decrease their inductance and limit the operating voltage, it is mandatory to use cables made up of several wires in parallel that are able to carry much larger currents, typically in the range of 10 kA. Such cables must ensure good current distribution through transposition, combined with precisely controlled dimensions necessary for obtaining coils of accurate geometry, as well as good winding characteristics. These properties are the characteristic of the flat cable invented at the Rutherford Laboratory in England [139].

Fig. 14. A Rutherford cable for the inner layer of the LHC dipoles, showing the Nb–Ti filaments in a few etched strands.

A typical Rutherford cable, shown in Fig. 14, is composed of fully transposed twisted wires (Nb–Ti in the figure). The rectangular geometry of the cable provides high strand packing and is flexible enough to wind magnet coils of various geometries. The transposition length, also referred to as the twist pitch, is usually kept short, of the order of a few centimeters. To improve the winding properties, the cable is slightly keystoned, i.e. the cable thickness is not constant from side to side. The angle formed by the planes of the cable upper and lower faces is called the keystone angle, which is usually in the range of 1°–2°. A summary of cable characteristics for the major superconducting accelerator projects is given in Table 1.

The cabling process is invariably associated with large deformations at the edges of the cable, where the wires are plastically deformed. This is necessary for achieving mechanical stability of the cable, but can lead to degradation of the critical current

Table 1. Main characteristics of the (bare) superconducting cables used to wind the dipoles for the four superconducting colliders.

Name	Strand diameter (mm)	Thickness (mm)	Width (mm)	Twist pitch (mm)	Keystone angle (degree)
Tevatron	0.68	1.26	7.8	66	2.1
HERA	0.90	1.48	10.0	95	2.2
RHIC	0.65	1.17	9.7	94	1.2
LHC inner	1.065	1.90	15.1	115	1.2
LHC outer	0.825	1.48	15.1	100	0.9

of the superconductor, as well as significant distortion of the diffusion barriers, or their breakage. The degradation can be divided into two origins: degradation associated with the intrinsic properties of the strand, and degradation due to the choice of cabling parameters.

The intrinsic properties of wires vary greatly, depending on the superconductor, as well as on the specific architecture. As an example, Nb–Ti strands are known to have good tolerance to deformation and cabling, while Nb_3Sn strands are less forgiving. Among strands based on the same superconducting material, architecture details such as filament size, position in the strand, and spacing are of the utmost importance. The intrinsic tolerance to cabling can be verified by tests such as the *sharp bend*, in which the wire is bent back sharply on itself in a fixture under controlled conditions, etched, and examined for broken filaments.

Cabling parameters that affect the amount of critical current degradation are mainly the amount of overall compaction, as well as other finer details, such as the cabling tension, the angle and shape of the cabling mandrel, the stability of the tooling, and the use of lubricants. Cable compaction depends on the thickness and width of the cabling cavity formed by the rollers placed at the cabling point of a typical machine. Following Ref. 140, we can define a thickness and width compaction (respectively c_t and c_w) as follows:

$$c_t = \frac{t}{2d} - 1, \tag{4}$$

$$c_w = \frac{w}{\left(\frac{Nd}{2\cos(\theta)}\right) + 0.72d} - 1, \tag{5}$$

where t is the cable thickness, w the cable width, d the strand diameter, N the number of strands in the cable, and θ the twist pitch angle. In addition, it is useful to define the overall cable compaction as follows:

$$c = (c_t + 1)(c_w + 1). \tag{6}$$

An acceptable compaction range for cabling of Nb–Ti strands is $c_t \approx -10\%$ to -15%, $c_w \approx -5\%$ to -10%, and $c \approx 80$–85%. Typical cabling degradation achieved in Nb–Ti cables manufactured in the above range is less than 5%. Such deformation, acceptable for Nb–Ti, is excessive for Nb_3Sn. For Nb_3Sn, it has been found empirically that the cable compaction should be limited to the range of 86% or larger. This should be considered as both an average and a local limit, to be respected specifically at the thin edge of a keystoned cable. Such a limit imposes very tight constraints on the range of feasible keystone angles, especially when producing wide cables for small-aperture magnets. In addition, and most important (as stressed in Ref. 140), compaction by itself does not guarantee a good final result. Indeed, the same compaction can be achieved by reducing either the width or the thickness, but the final result is very different in terms of cable degradation. It was found, again empirically, that for Nb_3Sn the preferred parameter range for cabling is $c_t \approx -5\%$ to -10% and $c_w = -3\%$ to 0%. Note how in this case the final width of the cable can exceed the theoretical cable dimensions, which is done intentionally to avoid excessive deformation at the thin edge, where the strands that transit from the upper to the lower face of a Rutherford cable are subjected to large deformations. This is in general satisfactory from the point of view of critical current degradation, which is typically limited to 5–10% of a virgin strand, but the resulting cable may not be sufficiently compacted to achieve the mechanical stability that is necessary for winding.

Despite the many years of experience, cabling is still a delicate balance between limited wire deformation and desired cable compaction. It depends on the specific material that is cabled as well as the

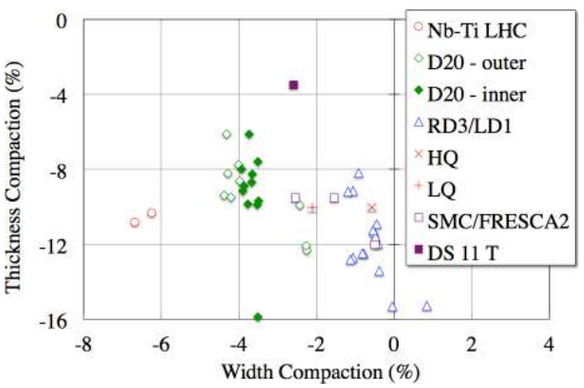

Fig. 15. Compilation of computed width and thickness compaction values for a number of cables manufactured in the past 10 years for Nb_3Sn applications, compared to the compaction of the LHC Nb–Ti cables. (Data for D20, RD3, HQ, LQ courtesy of D. Dietderich, LBNL; data for SMC, FRESCA2, DS 11 T courtesy of L. Oberli, CERN.)

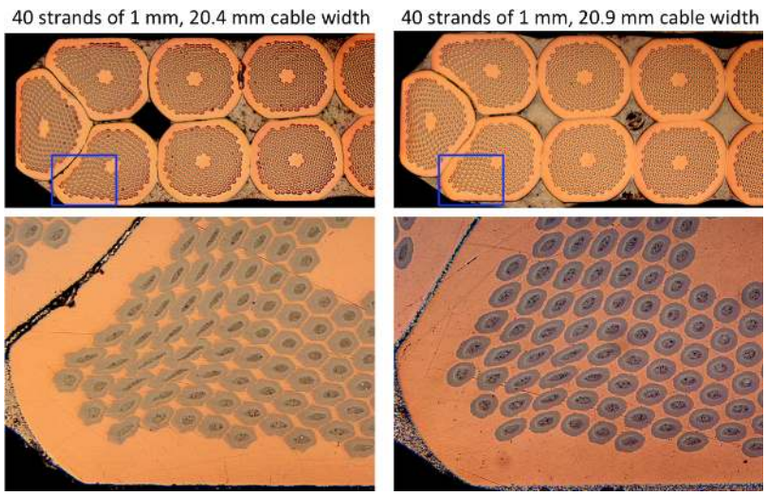

Fig. 16. Detail of the edge of prototype Rutherford cables built with PIT Nb_3Sn, 1-mm-diameter wires, with slightly different width (as indicated), identical thickness (1.82 mm), and twist pitch (120 mm). The area placed in the rectangles of the low-magnification micrographs is shown in the high-magnification images below. (Micrographs courtesy of A. Bonasia and L. Oberli, CERN.)

desired cable geometry, and the simple rules given above provide only a starting point for empirical optimizations. A collection of width and thickness compaction is reported in Fig. 15, showing how the realized Nb_3Sn cables tend to cluster in an area of reduced width deformation when compared to the LHC Nb–Ti cables. To illustrate the difficulty of such optimization, we show in Fig. 16 an example of cabling trials that have taken place during the development of a large-size Rutherford cable for the EuCARD magnet FRESCA-2. The cable, built with 40 PIT strands of 1 mm diameter, has a nominal dimension of 20.9 mm, a width of 1.82 mm, and a twist pitch of 120 mm. Micrographs of this cable, before heat treatment, are shown on the right hand side of the figure. They demonstrate that the local deformation at the most compacted location, the cable edge, is controlled to a tolerable level. Specifically, we observe no merging of subelements, and an acceptable reduction in the Nb thickness which guarantees that the Sn leakage and associated Cu poisoning during the heat treatment is small. On the other hand, as shown on the left hand side of the figure, a small reduction with respect to these optimized dimensions (a 2.5% reduction in the width) causes considerable deformation in the filaments and merging, which leads to degradation of J_c, a very low local RRR, and a large effective filament dimension.

The concept of Rutherford cables can be easily applied to any material that comes in the form of round wires, and it has been extended to round Bi-2212 HTS wires [113–116]. Further cable concepts, such as the Roebel bar, or tape assemblies around a stabilizer core or tube, discussed earlier, are in an early stage of development and have not yet found an accelerator application.

6. Summary

High-performance superconducting materials and conductors are the basic ingredient of the magnets for the large-scale accelerators that have been pushing the frontier of particle physics in the past 30 years. As we have discussed in this article, high critical current density is the principal, but not exclusive, target of such optimized conductors. While the presence is still largely dominated by the widespread use of Nb–Ti, literally the workhorse for all HEP applications to date, we predict that the next five years will be decisive for Nb_3Sn. A decennium of preparation has resulted in Nb_3Sn wires that are approaching the maturity necessary for HEP application, and the baton is now in the hands of the magnet builders whose task is to engineer solutions for the use of this upgraded material. At the same time, we hear HTS materials knock at the door. While priority is naturally, and rightly, given to Nb_3Sn, we believe that it is

important to continue the technological exploration of YBCO and Bi-2212. Fundamental questions need to be answered on the basic properties (critical current, mechanics), and the application in magnets (cables, protection) of these materials. Given the long time for such research, we stress the importance of national and international programs that are presently pursuing the construction of simple but very meaningful small-scale demonstrator magnets. In summary, the landscape of superconductors for HEP, and more generally accelerator applications, is varied and most interesting, with a number of opportunities and critical decision points approaching in the coming years. Superconductivity remains a fascinating field, from the enchantment of quantum physics on the microscopic scale, to the engineering challenge of the largest instrument ever built on the macroscopic scale.

Acknowledgments

The authors are grateful for the material and expertise provided by D. C. Larbalestier of the Applied Superconductivity Center at the NHMFL, Tallahassee, FL, USA; A. Ballarino, B. Bordini, L. Oberli, and D. Richter of CERN, Geneva, Switzerland; D. R. Dietderich of LBNL, Berkeley, CA, USA; and J. Schwartz of NCSU, Raleigh, NC, USA. This work was partly supported by the Director, Office of Science, High Energy Physics, US Department of Energy, under contract No. DE-AC02-05CH11231.

References

[1] H. Kolm, B. Lax, F. Bitter and R. Mills (eds.), *High Magnetic Fields: Proc. 1st Int. Conf. on High Magnetic Fields* (Cambridge, MA, USA; Nov. 1–4, 1961), p. 1662.
[2] J. E. Kunzler, *IEEE Trans. Magn.* **23**, 396 (1987).
[3] C. Laverick and G. M. Lobell, *Rev. Sci. Instrum.* **36**, 825 (1965).
[4] J. R. Purcell, The 1.8 tesla, 4.8 m I.D. bubble chamber magnet, in *Proc. 1968 Summer Study on Superconducting Devices and Accelerators* (Brookhaven National Laboratory, June 10–July 19, 1968), pp. 765–785.
[5] K. Jaeger and J. R. Purcell, Operation and accuracy of the 12-foot bubble chamber magnet, in *Proc. 4th Int. Conf. on Magnet Technology (MT4)* (Brookhaven National Laboratory, 1972), pp. 328–338.
[6] D. P. Brown, R. W. Burgess and G. T. Mulholland, The superconducting magnet for the Brookhaven National Laboratory 7-foot bubble chamber, in *Proc. 1968 Summer Study on Superconducting Devices and Accelerators* (Brookhaven National Laboratory, 1969), pp. 794–814.
[7] E. U. Haebel and F. Wittgenstein, Big European Bubble Chamber (BEBC) magnet progress report, in *Proc. 3rd Int. Conf. on Magnet Technology* (DESY, Hamburg, 1970), pp. 874–895.
[8] G. B. Yntema, *Phys. Rev.* **98**, 1197 (1955).
[9] G. B. Yntema, *IEEE Trans. Magn.* **23**, 390 (1987).
[10] J. E. Kunzler, E. Buehler, F. S. L. Hsu, B. T. Matthias and C. Wahl, *J. Appl. Phys.* **32**, 325 (1961).
[11] J. E. Kunzler, E. Buehler, F. S. L. Hsu and J. H. Wernick, *Phys. Rev. Lett.* **6**, 89 (1961).
[12] T. G. Berlincourt, *Cryogenics* **27**, 283 (1987).
[13] Rutherford Laboratory Superconducting Applications Group, *J. Phys. D* **3**, 1517 (1970).
[14] G. H. Morgan, *J. Appl. Phys.* **41**, 3673 (1970).
[15] R. R. Wilson *et al.*, The energy doubler design study: A progress report. Technical report (Fermilab, Batavia, IL, USA, 1974).
[16] A. Tollestrup, The Tevatron hadron collider: A short history, in *Int. Conf. on the History of Original Ideas and Basic Discoveries in Particle Physics* (Ettore Majorana Centre for Scientific Culture, Erice, Sicily, Italy; Jul. 29–Aug. 4, 1994).
[17] F. E. Mills, Isabelle design study, in *Proc. 1973 Particle Accelerator Conference* (1973), pp. 1036–1038.
[18] Central Design Group, SSC conceptual design report, Technical report (Central Design Group, 1986).
[19] D. E.-S. (Center), *HERA: A Proposal for a Large Electron–Proton Colliding Beam Facility at DESY* (Deutsches Elektronen-Synchrotron, 1981).
[20] G. Gurov, UNK status and plans, in *Proc. 1995 Particle Accelerator Conference* (Dallas, TX, USA, 1995), pp. 416–419.
[21] M. Anerella *et al.*, *Nucl. Instrum. Methods Phys. Res. Sect. A: Accelerators, Spectrometers, Detectors and Associated Equipment* **499**, 280 (2003).
[22] L. R. Evans and P. Bryant, *J. Instrum.* **3**, S08001, 164 (2008).
[23] L. Rossi and L. Bottura, *Reviews of Accelerator Science and Technology.*
[24] H. Desportes, *IEEE Trans. Magn.* **17**, 1560 (1981).
[25] M. A. Green *et al.*, *IEEE Trans. Magn.* **15**, 128 (1979).
[26] J. Benichou *et al.*, *IEEE Trans. Magn.* **17**, 1567 (1981).
[27] R. Wands *et al.*, *IEEE Trans. Magn.* **19**, 1368 (1983).
[28] J. M. Baze *et al.*, *IEEE Trans. Magn.* **24**, 1260 (1988).
[29] R. Apsey *et al.*, *IEEE Trans. Magn.* **21**, 490 (1985).
[30] H. H. J. ten Kate, *Physica C: Supercond.* **468**, 2137 (2008).

[31] A. Herve, *IEEE Trans. Appl. Supercond.* **10**, 389 (2000).
[32] R. M. Scanlan, *IEEE Trans. Appl. Supercond.* **11**, 2150 (2001).
[33] D. R. Dietderich and A. Godeke, *Cryogenics* **48**, 331 (2008).
[34] S. A. Gourlay, *IEEE Trans. Appl. Supercond.* **16**, 324 (2006).
[35] G. de Rijk *et al.*, *IEEE Trans. Appl. Supercond.* **22**, 4301204 (2012).
[36] P. J. Lee, private communication, http://magnet.fsu.edu/∼lee/plot/plot.htm (2012).
[37] Very High Field Superconducting Magnet Collaboration: A collaboration of groups at Brookhaven National Laboratory, Fermilab, Lawrence Berkeley National Laboratory, Los Alamos National Laboratory, the National High Magnetic Field Laboratory, North Caroline State University, and Texas A&M University seeking to understand and apply round wire Bi-2212.
[38] L. Bottura, L. de Rijk, G. Rossi and E. Todesco, *IEEE Trans. Appl. Supercond.* **22**, 4002008 (2012).
[39] A. Godeke, Performance boundaries in Nb_3Sn Superconductors. Ph.D. thesis (University of Twente, Enschede, The Netherlands, 2005).
[40] A. Ballarino, *IEEE Trans. Appl. Supercond.* **21**, 980 (2011).
[41] T. Ogitsu *et al.*, *IEEE Trans. Appl. Supercond.* **19**, 1081 (2009).
[42] L. Rossi and E. Todesco, *Phys. Rev. ST Accel. Beams* **10**, 112401 (2007).
[43] P. J. Lee and D. C. Larbalestier, *IEEE Trans. Appl. Supercond.* **15**, 3474 (2005).
[44] D. Leroy, L. Oberli, D. Perini, A. Siemko and G. Spigo, Design futures and performance of a 10 T twin aperture model dipole for LHC, in *Proc. 15th Int. Conf. on Magnet Technology* (Beijing, China, 1998), eds. L. Lianghzhen, S. Guoliao and Y. Lugang (Science Press, Beijing, China, 1998), Vol. 1, pp. 119–122.
[45] A. F. Lietzke *et al.*, *IEEE Trans. Appl. Supercond.* **14**, 345 (2004).
[46] M. N. Wilson, *Superconducting Magnets* (Oxord Science Publications, 1983).
[47] P. Ferracin *et al.*, *IEEE Trans. Appl. Supercond.* **15**, 1132 (2005).
[48] P. Ferracin *et al.*, *IEEE Trans. Appl. Supercond.* **16**, 378 (2006).
[49] A. Godeke, B. ten Haken, H. H. J. ten Kate and D. C. Larbalestier, *Supercond. Sci. Tech.* **19**, R100 (2006).
[50] D. Arbelaez, A. Godeke and S. O. Prestemon, *Supercond. Sci. Tech.* **22**, 025005 (2009).
[51] B. ten Haken, A. Godeke, H. J. Schuver and H. H. J. ten Kate, *IEEE Trans. Magn.* **32**, 2720 (1996).
[52] N. Cheggour *et al.*, *Supercond. Sci. Tech.* **25**, 015001 (2012).
[53] X. F. Lu *et al.*, *IEEE Trans. Appl. Supercond.* **22**, 8400307 (2012).
[54] N. Cheggour *et al.*, *Appl. Phys. Lett.* **83**, 4223 (2003).
[55] D. C. van der Laan *et al.*, *Supercond. Sci. Tech.* **23**, 014004 (2010).
[56] D. C. van der Laan *et al.*, *Supercond. Sci. Tech.* **23**, 072001 (2010).
[57] J. S. Higgins and D. P. Hampshire, *IEEE Trans. Appl. Supercond.* **21**, 3234 (2011).
[58] M. Sugano, K. Shikimachi, N. Hirano and S. Nagaya, *Supercond. Sci. Tech.* **23**, 085013 (2010).
[59] H. Boschman, A. P. Verweij, S. Wessel, H. H. J. ten Kate and L. J. M. van de Klundert, *IEEE Trans. Magn.* **27**, 1831 (1991).
[60] H. H. J. ten Kate, H. W. Weijers and J. M. van Oort, *IEEE Trans. Appl. Supercond.* **3**, 1334 (1993).
[61] J. M. van Oort, R. M. Scanlan, H. W. Weijers, S. Wessel and H. H. J. ten Kate, *IEEE Trans. Appl. Supercond.* **3**, 559 (1993).
[62] J. M. van Oort, R. M. Scanlan, H. W. Weijers and H. H. J. ten Kate, *Adv. Cryog. Eng. (Materials)* **40**, 867 (1994).
[63] D. R. Dietderich, R. M. Scanlan, R. P. Walsh and J. R. Miller, *IEEE Trans. Appl. Supercond.* **9**, 122 (1999).
[64] D. R. Dietderich *et al.*, *IEEE Trans. Appl. Supercond.* **11**, 3577 (2001).
[65] P. Bauer *et al.*, *IEEE Trans. Appl. Supercond.* **11**, 2457 (2001).
[66] J. W. Ekin, *IEEE Trans. Magn.* **MAG-23**, 1634 (1987).
[67] B. ten Haken and H. H. J. ten Kate, *Physica C* **270**, 21 (1996).
[68] B. ten Haken, A. Beuink and H. H. J. ten Kate, *IEEE Trans. Appl. Supercond.* **7**, 2034 (1997).
[69] D. Dell'Orco *et al.*, *IEEE Trans. Appl. Supercond.* **3**, 637 (1993).
[70] A. den Ouden, W. A. J. Wessel and H. H. J. ten Kate, *IEEE Trans. Appl. Supercond.* **7**, 733 (1997).
[71] A. D. McInturff *et al.*, Test results for a high field (13 T) Nb_3Sn dipole, in *Proc. 1997 Part. Accel. Conf.* (Vancouver, Canada, 1998), Vol. 3, pp. 3212–3214.
[72] E. Barzi, T. Wokas and A. V. Zlobin, *IEEE Trans. Appl. Supercond.* **15**, 1541 (2005).
[73] B. Seeber *et al.*, *IEEE Trans. Appl. Supercond.* **17**, 2643 (2007).
[74] B. Seeber, A. Ferreira, V. Abächerli and R. Flükiger, *Supercond. Sci. Tech.* **20**, S184 (2007).
[75] E. Barzi, D. Turrioni and A. V. Zlobin, *IEEE Trans. Appl. Supercond.* **18**, 980 (2008).
[76] B. Seeber *et al.*, *IEEE Trans. Appl. Supercond.* **18**, 976 (2008).
[77] P. Ferracin *et al.*, *IEEE Trans. Appl. Supercond.* **19**, 1240 (2009).

[78] G. Mondonico, B. Seeber, A. Ferreira, B. Bordini, L. Oberli, L. Bottura, A. Ballarino, R. Flkiger and C. Senatore, *Supercond. Sci. Tech.* **25**, 115002 (2012).
[79] H. Felice *et al.*, *IEEE Trans. Appl. Supercond.* **21**, 1849 (2011).
[80] J. K. Hulm and R. D. Blaugher, *Phys. Rev.* **123**, 1569 (1961).
[81] H. E. Cline, R. M. Rose and J. Wulff, Research on a superconducting Nb–Th eutectic alloy, Technical report: NASA Report CR 54103 (1964).
[82] H. E. Cline, B. P. Strauss, R. M. Rose and J. Wulff, *J. Appl. Phys.* **37**, 5 (1966).
[83] F. P. Levi, *J. Appl. Phys.* **31**, 1469 (1960).
[84] D. C. Larbalestier and P. J. Lee, New developments in niobium titanium superconductors, in *Proc. 1995 Particle Accelerator Conference and International Conference on High Energy Accelerators* (1996), pp. 1276–1281.
[85] J. D. Adam *et al.*, *IEEE Trans. Appl. Supercond.* **12**, 1056 (2002).
[86] J. D. McCambridge *et al.*, *IEEE Trans. Appl. Supercond.* **5**, 1697 (1995).
[87] E. Kadyrov, A. Gurevich and D. C. Larbalestier, *Appl. Phys. Lett.* **68**, 1567 (1996).
[88] M. N. Wilson, *Cryogenics* **48**, 381 (2008).
[89] M. N. Wilson *et al.*, "AC3" — a prototype superconducting synchrotron magnet, in *Proc. 1972 Appl. Supercond. Conf.* (May 1–3, 1972; Annapolis, MD, USA), eds. H. M. Long and W. F. Gauster, pp. 277–282.
[90] H. Brechna and M. A. Green, Pulsed superconducting magnets, in *Proc. 1972 Appl. Supercond. Conf.* (May 1–3, 1972; Annapolis, MD, USA), eds. H. M. Long and W. F. Gauster, pp. 226–238.
[91] G. Bronca, G. Neyret, J. Parain and J. Perot, Consequences of replacing conventional magnets by superconducting magnets in an existing synchrotron, in *Proc. 1972 Appl. Supercond. Conf.* (May 1–3, 1972; Annapolis, MD, USA), eds. H. M. Long and W. F. Gauster, pp. 283–287.
[92] T. Verhaege, Y. Laumond and A. Lacaze, *Handbook of Applied Superconductivity* (1998), p. 415.
[93] H. Krauth, *IEEE Trans. Magn.* **24**, 1023 (1988).
[94] G. Moritz, in *Proc. 2007 Particle Accelerator Conference* (Albuquerque, New Mexico, USA, 2007), p. 3745.
[95] B. T. Matthias, T. H. Geballe, S. Geller and E. Corenzwit, *Phys. Rev.* **95**, 1435 (1954).
[96] K. Tachikawa and P. J. Lee, History of Nb_3Sn and Related A15 Wires, in *100 Years of Superconductivity*, eds. H. Rogalla and P. H. Kes (CRC Press, 2012), Chap. 11.3.
[97] A. Godeke, *Supercond. Sci. Tech.* **19**, R68 (2006).
[98] M. G. Benz, *IEEE Trans. Magn.* **2**, 760 (1966).
[99] K. Tachikawa and Y. Tanaka, *Japan. J. Appl. Phys.* **5**, 834 (1966).
[100] M. T. Naus, Optimization of internal-Sn Nb_3Sn composites. Ph.D. thesis (Univ. of Wisconsin–Madison, 2002).
[101] V. Abächerli *et al.*, *IEEE Trans. Appl. Supercond.* **15**, 3482 (2005).
[102] A. Godeke *et al.*, *J. Appl. Phys.* **97**, 093909 (2005).
[103] A. Godeke, A. den Ouden, A. Nijhuis and H. H. J. ten Kate, *Cryogenics* **48**, 308 (2008).
[104] M. Suenaga, D. O. Welch, R. L. Sabatini, O. F. Kammerer and S. Okuda, *J. Appl. Phys.* **59**, 840 (1986).
[105] R. Flükiger *et al.*, *Supercond. Sci. Tech.* **21**, 054015 (2008).
[106] M. G. T. Mentink *et al.*, *Physics Procedia* **36**, 491 (2012).
[107] V. Kashikin and A. Zlobin, *IEEE Trans. Appl. Supercond.* **15**, 1621 (2005).
[108] B. Bordini, E. Barzi, S. Feher, L. Rossi and A. Zlobin, *IEEE Trans. Appl. Supercond.* **18**, 1309 (2008).
[109] B. Bordini and L. Rossi, *IEEE Trans. Appl. Supercond.* **19**, 2470 (2009).
[110] J. Parrell *et al.*, *IEEE Trans. Appl. Supercond.* **19**, 2573 (2008).
[111] M. Thoener, V. Abaecherli, A. Szulczyk, B. Lindenhovius, J. Sailer and K. Schlenga, presented at ICEC 24–ICMC 2012 (May 14–18, 2012; Fukuoka, Japan).
[112] A. Godeke *et al.*, *IEEE Trans. Appl. Supercond.* **17**, 1149 (2007).
[113] R. M. Scanlan *et al.*, *IEEE Trans. Appl. Supercond.* **9**, 130 (1999).
[114] T. Hasegawa *et al.*, *IEEE Trans. Appl. Supercond.* **11**, 3034 (2001).
[115] T. Hasegawa *et al.*, *IEEE Trans. Appl. Supercond.* **12**, 1136 (2002).
[116] A. Godeke *et al.*, *Supercond. Sci. Tech.* **23**, 034022 (2010).
[117] H. Miao *et al.*, *IEEE Trans. Appl. Supercond.* **17**, 2262 (2007).
[118] H. Miao, Y. Huang, M. Meinesz, S. Hong and J. Parrell, *Adv. Cryog. Eng. (Materials)* **58**, 315 (2011).
[119] H. Weijers *et al.*, *IEEE Trans. Appl. Supercond.* **20**, 576 (2010).
[120] A. Godeke *et al.*, *Physics Procedia* **36**, 812 (2012).
[121] F. Kametani *et al.*, *Supercond. Sci. Tech.* **24**, 075009 (2011).
[122] Bi-2212 Strand and Cable Collaboration: A collaboration of groups at Brookhaven National Laboratory, Fermilab, Lawrence Berkeley National Laboratory, and the National High Magnetic Field Laboratory, seeking to understand and apply round wire Bi-2212.
[123] J. Jiang *et al.*, *Supercond. Sci. Tech.* **24**, 082001 (2011).
[124] T. Sekitani *et al.*, *Physica C* **392–396**, 116 (2003).

[125] T. Sekitani, N. Miura, S. Ikeda, Y. H. Matsuda and Y. Shiohara, *Physica B* **346–347**, 319 (2004).
[126] T. Sekitani, Y. H. Matsuda and N. Miura, *New J. Phys.* **9**, 47 (2007).
[127] D. C. Larbalestier, The long road to high current density superconducting conductors, in *100 Years of Superconductivity*, eds. H. Rogalla and P. H. Kes (CRC Press, 2012), Chap. 11.1.
[128] J. L. MacManus-Driscoll *et al.*, *Nat. Mater.* **3**, 439 (2004).
[129] A. Xu *et al.*, *Supercond. Sci. Tech.* **23**, 014003 (2010).
[130] V. Braccini *et al.*, *Supercond. Sci. Tech.* **24**, 035001 (2011).
[131] A. Gurevich, *Supercond. Sci. Tech.* **20**, S128 (2007).
[132] Bruker-EST, YBCO Coated Conductor Data Sheet (2012).
[133] W. Goldacker *et al.*, *Supercond. Sci. Tech.* **22**, 034003 (2009).
[134] S. Schlachter, W. Goldacker, F. Grilli, R. Heller and A. Kudymow, *IEEE Trans. Appl. Supercond.* **21**, 3021 (2011).
[135] N. Long, R. Badcock, K. Hamilton, A. Wright, L. Jiang and Z. Lakshmi, *J. Phys. Conf. Ser.* **234**, 022021 (2010).
[136] J. Fleiter, A. Ballarino, L. Bottura and P. Tixador, *Supercond. Sci. Tech.*, submitted for publication (2012).
[137] D. C. van der Laan, X. F. Lu and L. F. Goodrich, *Supercond. Sci. Tech.* **24**, 042001 (2011).
[138] L. Ye, F. Hunte and J. Schwartz, Stability and quench behavior of $Bi_2Sr_2CaCu_2O_x$ coils at high magnetic fields. Private communication (2012).
[139] G. Gallagher-Daggit, Superconductor cables for pulsed dipole magnets. Technical report (Rutherford Laboratory Memorandum No. RHEL/M/A25, 1973).
[140] D. R. Dietderich, N. L. Liggins and H. C. Higley, Development of high current Nb_3Sn Rutherford cables for NED and LARP. Private communication (2008).

Arno Godeke was educated in Mechanical Engineering and Applied Physics in The Netherlands. He has broad multidisciplinary experience in mechanical, electrical, and cryogenic design, fabrication, and implementation; and, in materials science, large-scale applications and the physics of superconductors. He has worked in superconductivity in various positions at the University of Twente, The Netherlands, from 1992 through 2005. In 1998, he visited the NHMFL, Tallahassee, FL, USA, on a sabbatical, and worked at the University of Wisconsin, Madison, WI, USA, from 2002 to 2003 to obtain his PhD in Applied Physics from Twente in 2005. Since 2006, Dr. Godeke is at LBNL, Berkeley, USA, where he is responsible for the conductor support for LBNL's high-field magnets and LARP, the development of new high-field technologies, and fundamental research through the education of young talent.

Luca Bottura is a Nuclear Engineer at the Engineering Faculty of the University of Bologna (Italy), and has received a PhD from the University College of Swansea (Wales, UK) for the physical modeling, scaling and numerical analysis of quench in large force-flow cooled superconducting coils. After nine years of experience in the design and testing of superconducting cables and magnets for fusion (NET and ITER), he joined CERN in 1995, where he initially supervised field mapping activities for the LHC magnets, and devised the Field Description for the LHC (FiDeL), an embedded system of the LHC controls. As of July 2011, he is the leader of the MSC group in the CERN Technology Department, in charge of the resistive and superconducting magnets for the CERN accelerator complex, the associated manufacturing and test technologies, and installations.